UCLouvain

epl

École polytechnique de Louvain

Design of an all-metal antenna array for space application

Author: **Pauline VRYGHEM**
Supervisor: **Christophe CRAEYE**
Readers: **Fisette PAUL, Al Khalifeh KHALDOUN**
Academic year 2022–2023
Master [120] in Electrical Engineering

Abstract

The exploration of the interior, and thus the origin of the planets and moons has always been of major scientific interest because of its intimate link to our own existence.

This master thesis takes place in the continuation of the LaRa (Lander Radio science) project which aims at collecting informations on the rotation and the orientation of Mars using radiosciences.

In that context, this work serves as a building block for the study of the interior properties of Triton, the biggest moon of Neptune. Among the numerous moons of the solar system, Triton is particularly interesting for several reasons. First, it may host an internal ocean and consequently be a potential source of life. Second, Triton is the only moon of the solar system orbiting in a retrograde direction.

Given the large distance between Triton and the Earth, the most realistic scenario consists of using an orbiter around Neptune which serves as a relay between a lander on Triton and the Earth.

This master thesis focuses on the design of the antenna to be mounted on the Triton lander. First, based on the Esa *Ice Giants* study report, informations about the orbiter, the space environment, the lander payload, etc. have been collected. Second, an analysis of two potential orbits, namely the equatorial orbit and the polar orbit, has been carried out. This study serves also as a basis for the link budget analysis. Relying on the link budget and on the required Signal to Noise Ratio (SNR), the antennas specifications are derived. Third, two antenna arrays are proposed, one for each orbit. The antennas are built of metal only so as to withstand to the harsh environment of Triton. Finally, the impact of the designed antenna on the link budget is closely analyzed, showing that a good communication can be established during almost the entire orbit.

Remerciements

Je souhaite remercier mon superviseur Prof. Christophe Craeye pour le suivi apporté à mon mémoire ainsi que le temps qu'il m'a accordé pour répondre à toutes mes questions tout au long de ce travail.

Je souhaite également chaleureusement remercier Laetitia Niyonzima et Modeste Bodehou pour tout le soutien, la gentillesse et l'aide apportés.

Je remercie également Véronique Dehant, Sébastien Le Maistre et Valerio Filice de l'Observatoire royal de Belgique pour les précieuses informations apportées à ce travail.

Enfin, je remercie mes proches pour leur soutien.

Contents

List of Figures

Chapter 2

Chapter 3

Chapter 4

Chapter 5

Chapter 6

Chapter 7

Chapter 8

Acronyms

AOGNC Attitude and Orbit Guidance, Navigation and Control. 6

DHS Data Handling System. 6

ESA European Space Agency. 4

ET Eastern Time. 8

NASA National Aeronautics and Space Administration. 4

ORB Observatoire Royal de Belgique. 8

PCDU Power Conditioning And Distribution Unit. 6

SNR Signal to Noise Ratio. 3, 16, 17

Chapter 1

Introduction

In 1612, Galileo discovered Neptune, but for the reason that its orbital revolution was very long, he catalogued it as a fixed star rather than a planet. The 4 498 400 000 km semi major axis of its orbit makes it the farthest planet from the Sun, an "Ice Giant" evolving in an obscure and bitter world [1].

At Neptune's surface, the solar irradiance has a magnitude of approximately $1.5\,\mathrm{W\,m^{-2}}$, leaving the celestial body in a never-ending dusk characterized by a luminosity a thousand times lower than the one at the surface of the Earth. With the pecularity to radiate 2.61 times more energy than it receives, Neptune surface temperature stalls at 60 K while its thermosphere reaches 750 K [2]. This element provides evidence of another heat source besides solar irradiation, possibly disturbing electromagnetic signals in the surrounding of the planet.

Its apparent magnitude (a measure of its irradiance from Earth) oscillates between 7.6 and 8, making it inaccessible for observation without instruments [3]. The extreme conditions of Neptune raises numerous challenges for a mission around it, among which energy management is not the least, starting with the storage and transport over a 15 years travel through the deep cold of space [4]. Energy limitations also constraint consuming devices to operate at strictly limited regimes, with the highest efficiency.

More specifically, in this work, the interest is towards the understanding of the interior of Triton, the biggest moon of Neptune. Table 1.1 compares some characteristics of our moon with that of Triton. Triton is a particular moon because it has the unique characteristic of orbiting in the retrograde direction around Neptune, the explanation to this fact could be that it has been captured from the Kuiper belt. Triton's surface is covered by a solidified nitrogen layer at the temperature of 38 K,

it stands out as the coldest location in the solar system [5]. The study of Triton, is in the same line as the LaRa (Lander Radio science) [6] which aims at study the interior of Mars [7]. However, in opposite to the Lara mission where a direct link is established between the Earth and a Mars lander, here an orbiter around Neptune is used as a relay between a Triton lander and the Earth. Indeed, Neptune is the furthest planet of the solar system, which makes the distance between Triton and the Earth significantly large (about 4.3 billions kilometers [8]).

Among the multiple challenges (mechanical, energetic, etc.), the telecommunication system constitutes a critical factor of the mission's success. Indeed, its role consists of collecting and reporting data for the sensing of the planet/moon of interest.

The purpose of this master thesis is to design an antenna positioned on a lander at the surface of Triton, and communicating with a Neptune orbiter. The antenna will serve to transmit signals containing useful informations on Triton's rotation, on the tides, etc. through Doppler measurement. Space antenna design is very complex because of the strong requirements resulting from the harsh space environment [9], [10]. Indeed, the antenna has to operate at extreme temperatures, and supports high cosmic radiations. Given those requirements, the antenna proposed in this thesis is built using metal only. In particular, an array of 8 metal radiators is proposed for the two considered orbits. The numerical analysis of the proposed antenna along with the link budget analysis allows us to prove that a good communication link can be established between the lander and the orbiter in almost the entire orbit.

	Triton	Earth's Moon
Average orbit distance [km]	354759	384400
Mean orbit velocity [km/h]	15803.2	384400
Orbit eccentricity [/]	0	0.0554
Equatorial radius [km]	1353.4	1737.5
Equatorial circumference [km]	8503.7	10917
Volume [km^3]	1.03 $10^1$0	2.2 $10^1$0
Density [g/cm^3]	2.059	3.344
Mass [kg]	21.39 10^{21}	73.48 10^{21}
Surface area [km^2]	23.02 10^6	37.93 10^6
Surface gravity [m/s^2]	0.779	1.624
Escape velocity [km/h]	5229	8552

Table 1.1: From [11], comparison table of Triton and Earth's moon characteristics.

The thesis is organized around 9 chapters. The first chapter introduces the work and presents the goals. The second chapter provides the useful informations on the

orbiter gain, the atmospheric losses, the lander payload, etc. Those informations are extracted from the *Ice Giants* study report [12]. The third chapter analyzes various orbit configurations. Then, Chapter 4 studies the link budget and provides a parametric study of the Signal to Noise Ratio (SNR). Thereafter, Chapter 5 relies on the previous ones to derive the antenna requirements. Afterwards, the sixth to the eighth chapters are devoted to the antenna design and the analysis of its impact on the link budget. Finally, Chapter 9 concludes the thesis.

Chapter 2

Analysis of the Esa study report "Ice Giants"

« Ice Giants » [12] is the study of a potential exploration mission for Uranus, for Neptune and its main moon Triton. The launch has been fixed to 2031 in order to take advantage of a "Jupiter Swing-by" and to put the two orbiters of the NASA (for Uranus) as well as the one of the ESA (for Neptune) on their respective trajectories. Figure 2.1 illustrates this scenario, the X-Y plane represents the ecliptic plane. The journey to Neptune lasts for approximately 15 years. The analysis of the *Ice Giants* report [12] allows one to better understand the stakes of such a mission, to find some specifications or orders of magnitude needed for this kind of antenna. The Doppler experience for which the antenna is designed in this work is not described in this document.

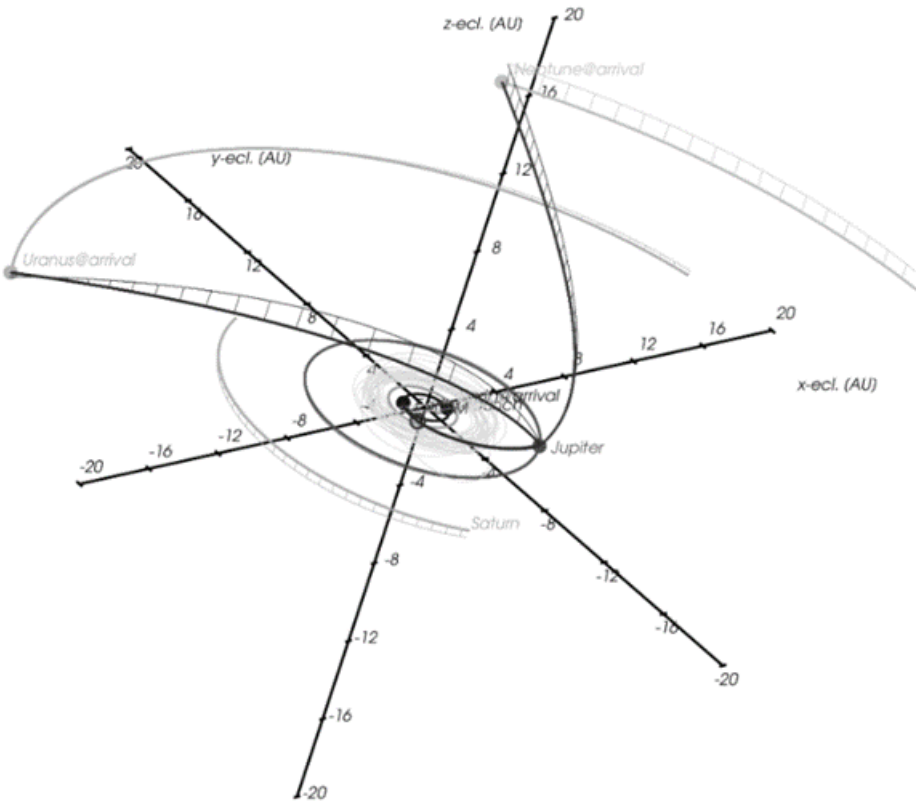

Figure 2.1: Trajectories of a NASA orbiter and an ESA orbiter reaching their respective planet Uranus and Neptune. The orbiters take advantage of a doable Jupiter swing-by in 2031 [12].

2.1 Objectives of the mission to Triton

Priority #1(the highest priority):

- Mapping of the surface geology at the landing site
- In situ surface and subsurface characterisation.

Priority #2:

- Determining the surface composition , including organic matter

– Describing the mass exchange/volatile transport

– Determining the composition of Triton's atmosphere

Priority #3:

– Studying moon-magnetosphere interactions

2.2 Requirements for the Triton lander communicating system

The lander studied in the *Ice Gnts* mission [12] is a lander of one week lifetime which is supposed to be released in the atmosphere from Triton fly-by (and not from a Triton orbit). The landing site is not indicated.

Mass budget The reduction of the antenna weight is a fundamental element to take into account. Indeed, the mass budget can not exceed 12.31 kg for the communications and 11.18 kg for the scientific instruments.

Power The minimal conceivable power budget is a 70 W peak power, which is distributed between the different units as detailed in Table 2.1. They then dispose of a 20 W of RF power for communication. PCDU is the Power Conditioning And Distribution Unit, DHS is the Data Handling System and AOGNC is for Attitude and Orbit Guidance, Navigation and Control.

Unit	Power [W]
PCDU	10
DHS	20
AOGNC	20
Communication	20

Table 2.1: Power distribution on the Triton lander.

Atmospheric losses The atmospheric losses in the case of an X-band link are assumed to be of 12 dB. This value is in fact the best estimation for Neptune atmospheric losses experienced by an atmospheric probe released in the Neptune atmosphere. The autors of [12] assume the Triton atmospheric losses to be the same.

Orbiter The assumptions made concerning the spacecraft communicating in the X-band are

- The orbiter gain is of the order of 40 dB gain at 8.45 GHz with a minimum antenna aperture of $1.5^2\pi$ m^2.
- A noise temperature of 1000 K is the worst case experimented by the orbiter receiver.

2.3 Summary

The Table 2.2 lists the useful information that we find in this study report for the X-band antenna design.

Scientific instrument's mass budget [kg]	11.18
Power [W]	20
Triton atmospheric losses [dB]	12
Orbiter gain [dB]	~ 40
Worst case noise temperature [K]	1000

Table 2.2: Useful communication system parameters of the *Ice Giants* mission Triton lander.

Chapter 3

Orbital Configurations

3.1 Type of orbit

In this work, a Neptunian orbit appears to be the most reasonable choice as it encompasses the whole planet-moon system and consequently also enables observations on Neptune.

For the scientific experiment, the analysis of different tracking geometries is essential in understanding which one provides the most useful information. One should also note that, according to the Royal Observatory of Belgium (ORB), when the spacecraft is high in the sky, i.e. for high elevations, the Doppler signature of the libration is the strongest. The libration refers to the slight oscillation of a celestial body as it is orbiting around another body [13]. In this work, we limits ourselves to two types of Neptunian orbits: an equatorial orbit and a polar orbit. The orbits are in 1:2 resonance with Triton, which means that when Triton has made one period of revolution, the orbiter has made two. It is important to underline that a resonant orbit may not be the best scenario because it shows repetitive geometries.

The position of the lander on Triton is also an important parameter affecting the quality of the geophysical signal. Within this work, we decide to limit the analysis to a lander placed on the Triton equator and in front of Neptune.

The simulations of the orbits are provided by the Royal Obervatory of Belgium (ORB). We have at our disposal the relative trajectory of the orbiter with respect to the lander during a time span of [01-JAN-2020 00:00:00 ET : 14-JAN-2020 00:00:00 ET]. The geometry of the orbits is assumed to be constant in time because the

underlying model does not take any perturbations (e.g. solar pressure, relativistic effects, etc) into account. Additionally, Triton has been modeled as a sphere of radius 1352.6 km. The coordinates are referenced with respect to a topocentric frame at a local point on the surface body. The frame center corresponds to the chosen lander position. The latter is defined by the geodetic heigth (always equal to zero as it is on the Triton surface), the lander latitude and longitude. Figures 3.1 and 3.2 show two representations of this frame, which is fixed at a zero longitude and latitude. As it can be seen, the zenith direction is the z-axis, the x-axis and the y-axis point to the north and the west respectively. The x- and y-axes form a plane tangent to the equator of Triton.

In particular, the variables describing the trajectory of the orbiter relative to the lander are:

- The time (in seconds [s]): computed from a time reference corresponding to the 01-JAN-2020 00:00:00.
- The elevation angle θ_c (in degrees [°]): angle between the xy-plane and the direction of observation. The complementary angle of the elevation (θ) is defined as $\theta = 90° - \theta_c$. One should note that θ_c=90° corresponds to a direction of observation pointing towards Neptune. Similarly, a negative value of θ_c means that the orbiter is behind Triton.
- The azimuth angle ϕ (in degrees [°]): angle between the x-axis and the projection of the direction of observation in xy-plane.
- Range (in kilometers [km]): relative distance between the orbiter and the system of reference on the lander.

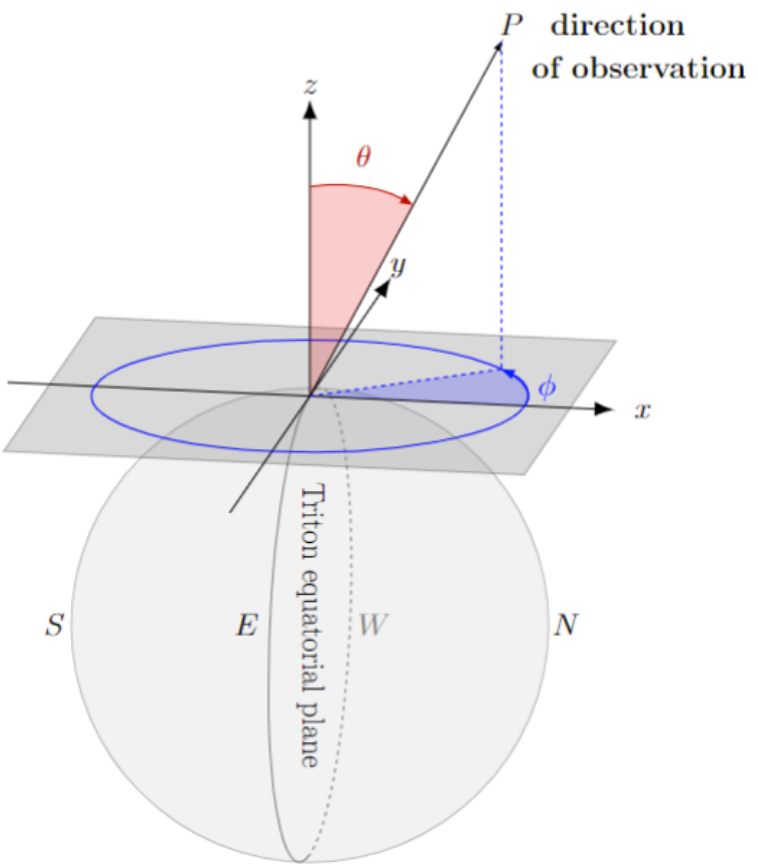

Figure 3.1: Topocentric frame attached to the Triton lander. The sphere is Triton. The North N, the South S, the East E and the West W are indicated.

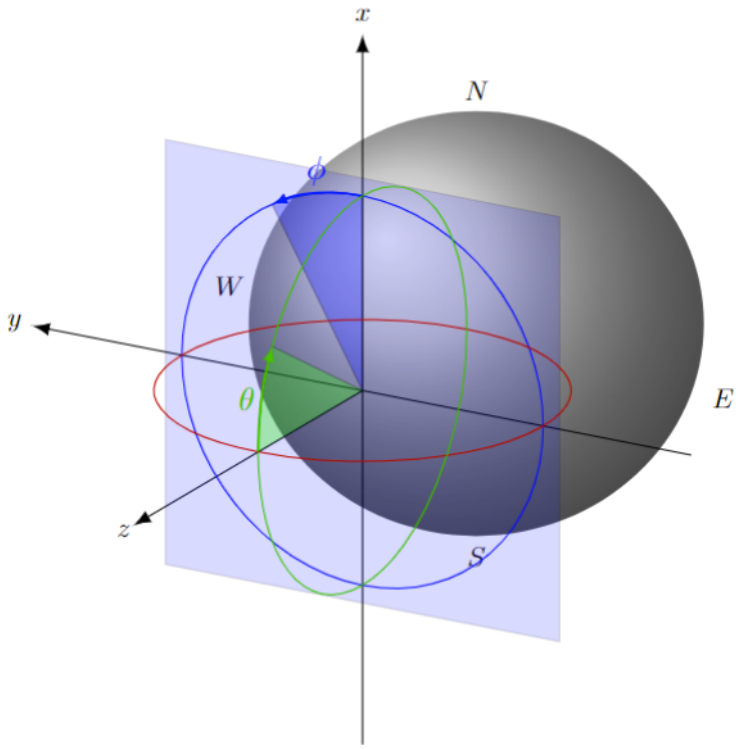

Figure 3.2: Topocentric frame attached to the Triton lander. The grey sphere represents Triton. The North N, the South S, the East E and the West W are indicated. The red circle lies in the equatorial plane of Triton.

3.2 The equatorial orbit

In this case, the orbital plane coincides with the equatorial plane. Therefore, the scenario can be analyzed in a 2D plane as represented in Figures 3.3 (a) and (b).

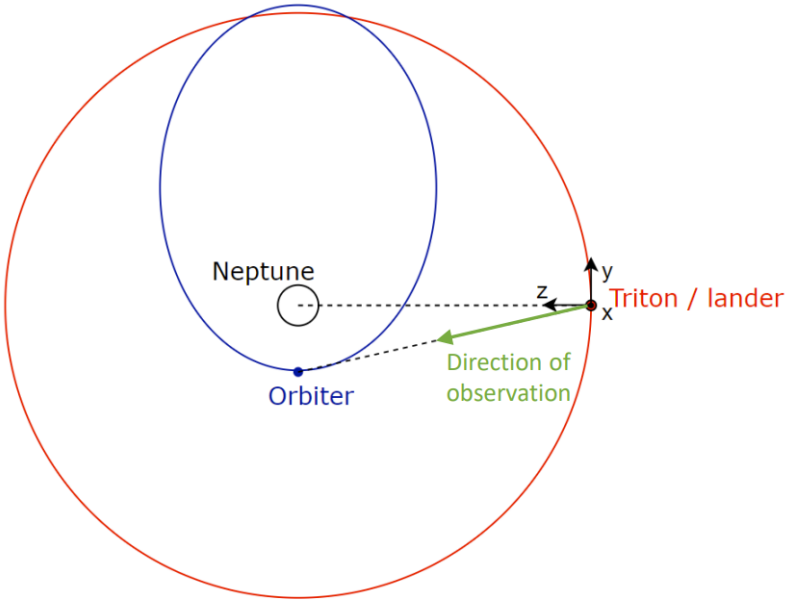

Figure 3.3: Equatorial orbit. In red: Triton's trajectory. In blue: orbiter's trajectory. The Cartesian system of reference xyz is attached to Triton.

The elevation θ_c, the azimuth ϕ, and the range are plotted in Figure 3.4. As expected, a binary behavior of the azimuth is observed ($\phi \in \{ 90°, 270°\}$), confirming that the trajectory of the orbiter is in the equatorial plane of Triton. Furthermore, it can be observed that when the range is minimum, θ_c= -90°, then attesting that the lander is facing Neptune.

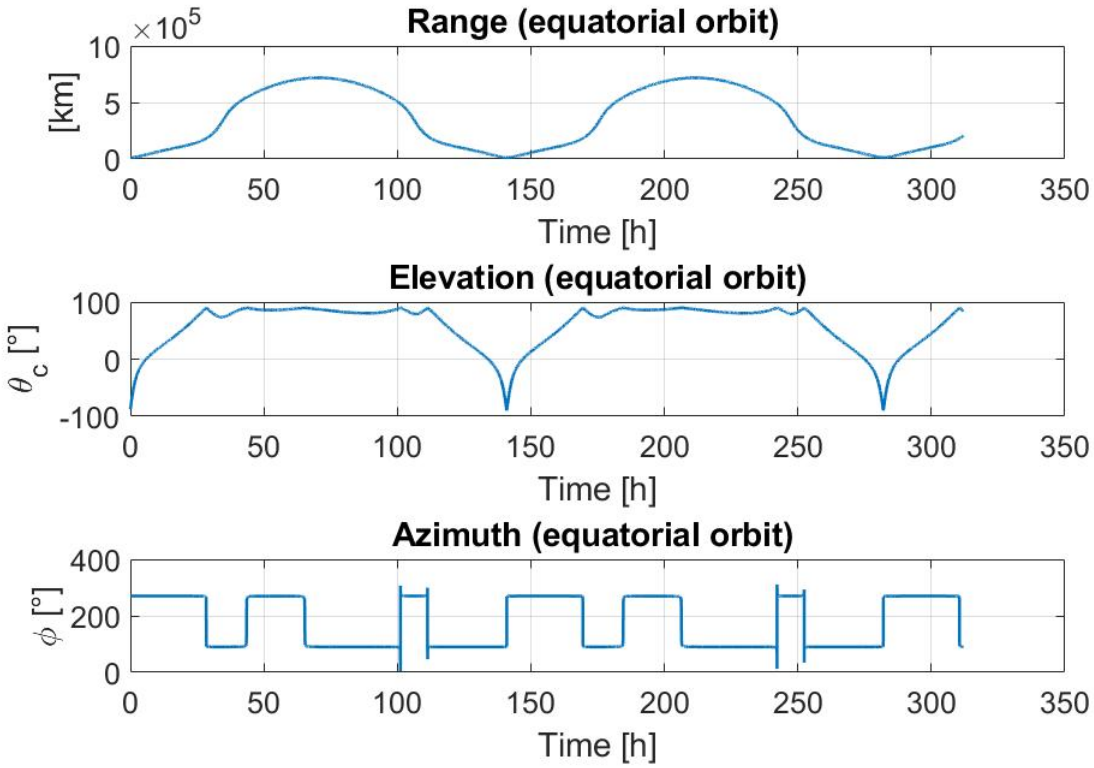

Figure 3.4: Range, elevation and azimuth for the equatorial orbit.

3.3 The polar orbit

The polar orbit of the spacecraft lies in a plane perpendicular to the equatorial plane as shown in Figure 3.5. The evolution of the azimuth, elevation and range as a function of time for the polar orbit is represented in Figure 3.6. As observed, the elevation becomes negative when the lander and the orbiter are at the closest, meaning that the lander is facing Neptune.It is worth mentioning that, in opposite to the equatorial orbit, here the azimuth no longer has a binary behavior.

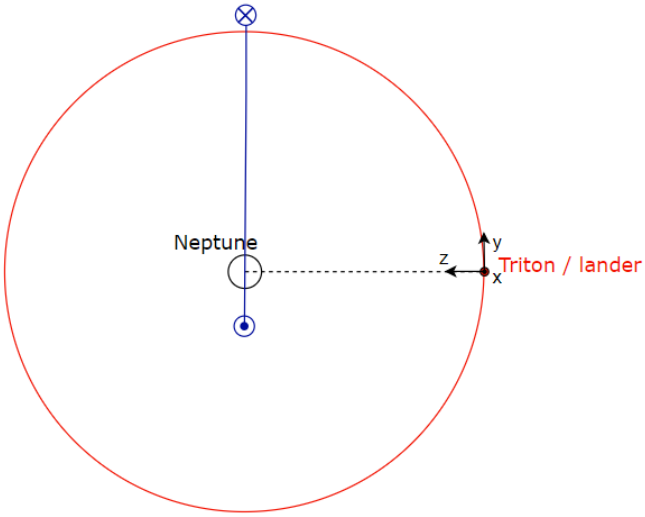

Figure 3.5: Polar orbit. In red: Triton's trajectory. In blue: orbiter's trajectory. The Cartesian system of reference xyz is attached to Triton.

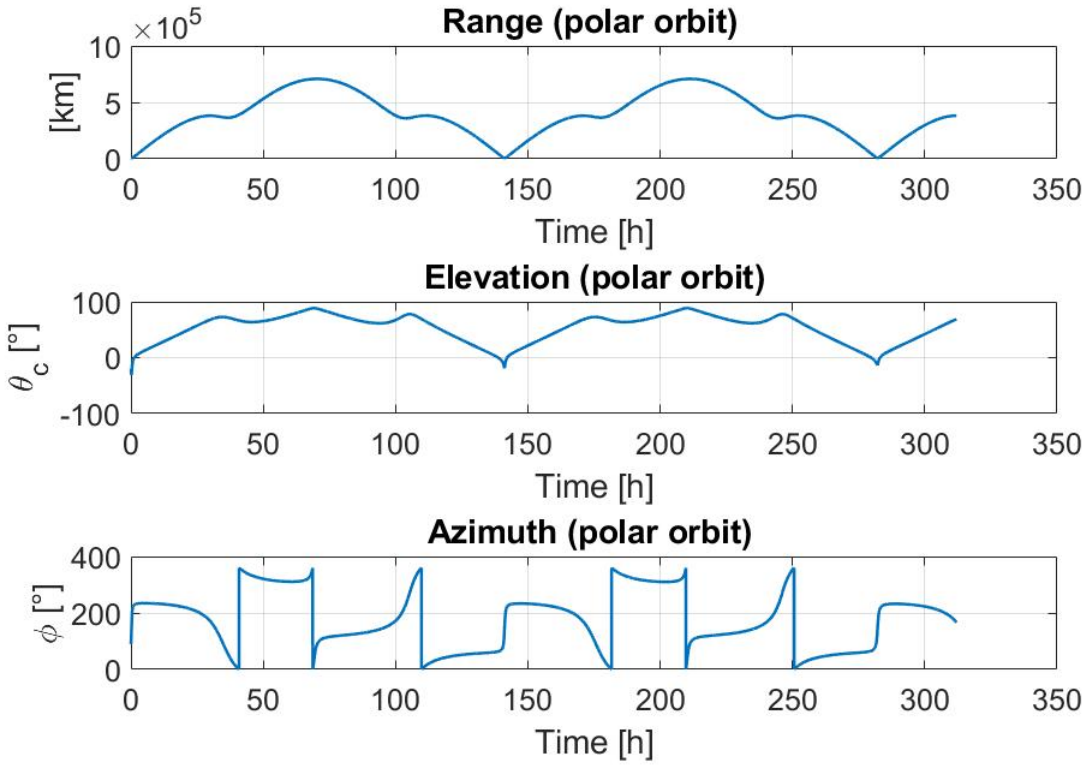

Figure 3.6: Range, elevation and azimuth for the polar orbit with a lander at latitude zero and longitude zero

Chapter 4

Link Budget

The purpose in this chapter is to establish the link budget in order to analyze the quality of the communication between the lander and the orbiter. The communication quality is quantified with the Signal to Noise Ratio (SNR), which can be expressed as :

$$SNR = G_T + P_T + G_R - L_{FS} + L_{ATM} - kB - T_S + M + 10\log_{10}(\sin\theta). \quad (4.1)$$

In equation (4.1) :

- SNR is the Signal to Noise Ratio in dB.
- G_T is the transmitted antenna gain in dBi.
- P_T the transmitted power in dB.
- G_R the received antenna gain in dBi.
- L_{FS} is the free-space loss in dB.
- L_{ATM} is the atmospheric loss in dB.
- k and B are the Boltzmann constant and the noise bandwidth respectively, with kB expressed in dB.
- T_S the system noise temperature in dB.
- M a security margin

- θ is the elevation of the orbiter with respect to the lander in a reference frame attached to the lander. The corresponding term models the signal degradation at grazing angles.

Among these parameters, some are fixed and other will be subject to a parametric study analysis.

4.1 Transmission gain and transmission power

The transmitting gain and the transmitting power are not fixed; they have to be adjusted to provide a sufficient SNR. Nonetheless, based on the ESA document [12], it can be assumed a maximum power of 20 W. Obviously, the lower the power, the better it is for lander energy savings.

4.2 Receiver gain

The receiver gain is the gain of the orbiter. Considering a receiving antenna with efficiency η_A and surface S, the gain can be written as:

$$G_R = 10 \log_{10} \left(\eta_A \left(\frac{S}{\lambda^2} \right) \right) \tag{4.2}$$

In this work, G_R is fixed to a value of 40 dBi as provided by the ESA study report [12] for X-Band communication.

4.3 Free-space and atmospheric losses

The free-space loss is due to the spread out of a finite power density over an increasing spherical surface. It varies with the range and represents a major contribution to the losses. It is given by:

$$L_{fs} = \left(\frac{4\pi r}{\lambda} \right)^2 \tag{4.3}$$

Regarding the atmospheric losses, we consider the ESA approximation of 12 dB in the X-Band.

4.4 Noise power

The noise power is given by :

$$N = kBT_S \tag{4.4}$$

4.4.1 Noise bandwidth

It is known that due to the Doppler effect, the received signal may vary in a large frequency band given by (4.5).

$$B_{max} = v_{r_{max}} \frac{f}{c} \tag{4.5}$$

where v_{rmax} is the maximum relative radial velocity, f is the operating frequency and c is the velocity of light.

A first way to estimate the noise bandwidth may be based on B_{max}. However, in practice, a bandpass filter of 30 Hz is implemented to sweep and lock on the instantaneous frequency of the receiving signal. Using this filter, one may consider the noise bandwidth as equal to B_{min}=30 Hz.

In practice, none of the previous models is strictly valid. A third approach may consist of using the logarithmic mean ($B_{average}$) between B_{max} and B_{min}.

Table 4.1 summarizes the noise bandwith of each orbit.

	B_{min}	$B_{average}$	B_{max}
Equatorial	0.03	2.975	295.02
Polar	0.03	2.0881	145.34

Table 4.1: Bandwidth in kHz selected for the parametric study

4.4.2 Noise temperature

ESA assumes a worst case noise temperature of 1000 K [12], which may seem very high as compared to other well known reference values. Other sources, like

[14] suggest a noise temperature around 200 K. The exact noise temperature is between 200 K and 1000 K depending on the proportion of the antenna field of view intercepted by Neptune. Considering that Neptune is viewed from the lander over an angle 2β with a beamwidth 2α (see Figures 4.1 and 4.2).

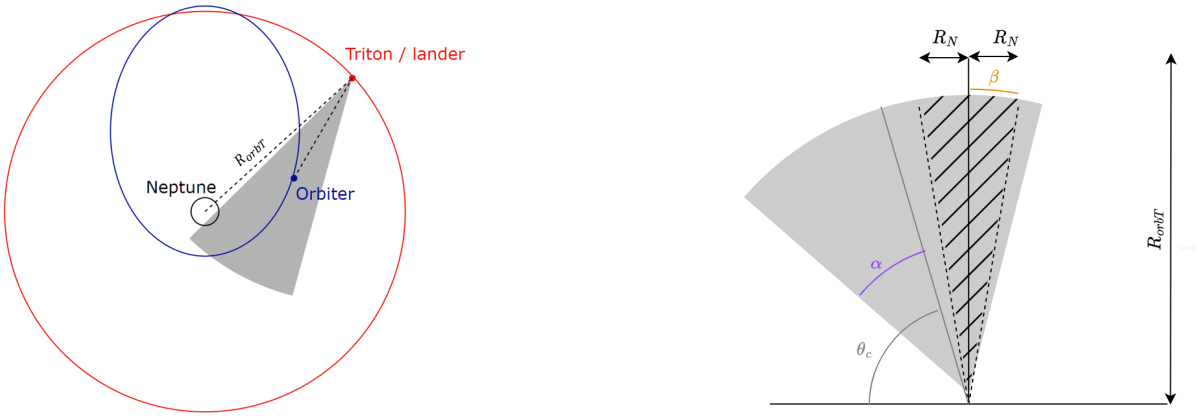

(a) (b)

Figure 4.1: Illustration of the coverage when the beam angle is fully encompassing Neptune. R_{orbT} is the radius of the Triton's orbit around Neptune and R_N is the radius of Neptune.

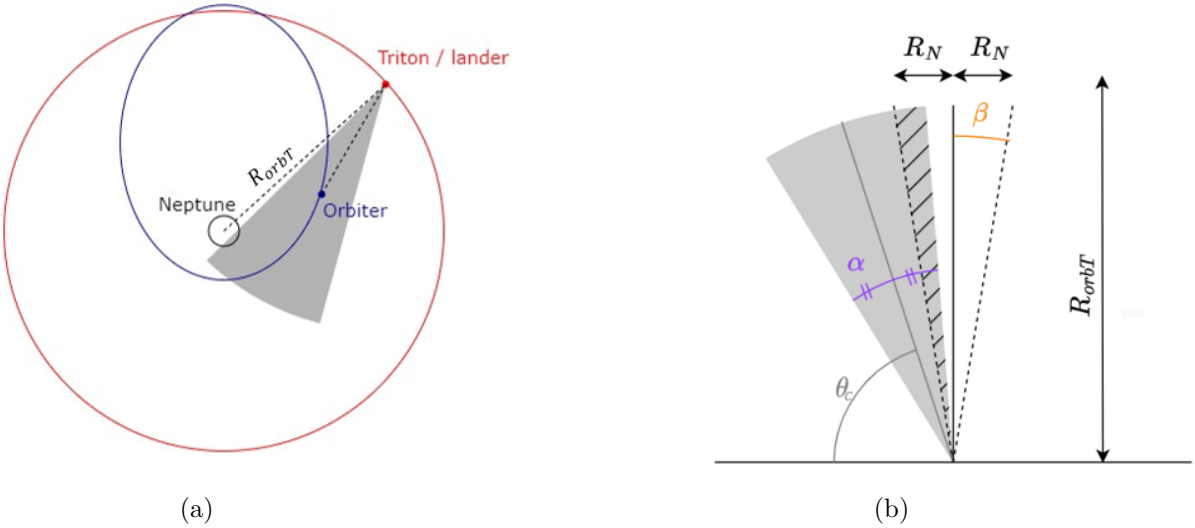

(a) (b)

Figure 4.2: Illustration of the coverage when the beam angle is partially encompassing Neptune. R_{orbT} is the radius of the Triton's orbit around Neptune and R_N is the radius of Neptune.

α and β can be estimated as :

$$\alpha = \frac{160}{2\sqrt{G_t}} \tag{4.6}$$

$$\beta = \arctan \frac{R_N}{R_{orbT}} \tag{4.7}$$

A linear model of the system temperature T_S is then proposed :

$$T_S = 200 + \tau 800 \tag{4.8}$$

where τ is defined as the ratio between the hatched area angle covered by Neptune and the field of view of the antenna beam.

Figure4.3 shows the coverage rate over time for different gains in the case of an equatorial orbit. We observe that for gains ranging from 2 dBi to 11 dBi, τ is constant over time. It is because the beam is sufficiently large to always fully intercept Neptune. However, for a gain of 14 dBi, we observe a variation of τ over time due to the beam being narrower.

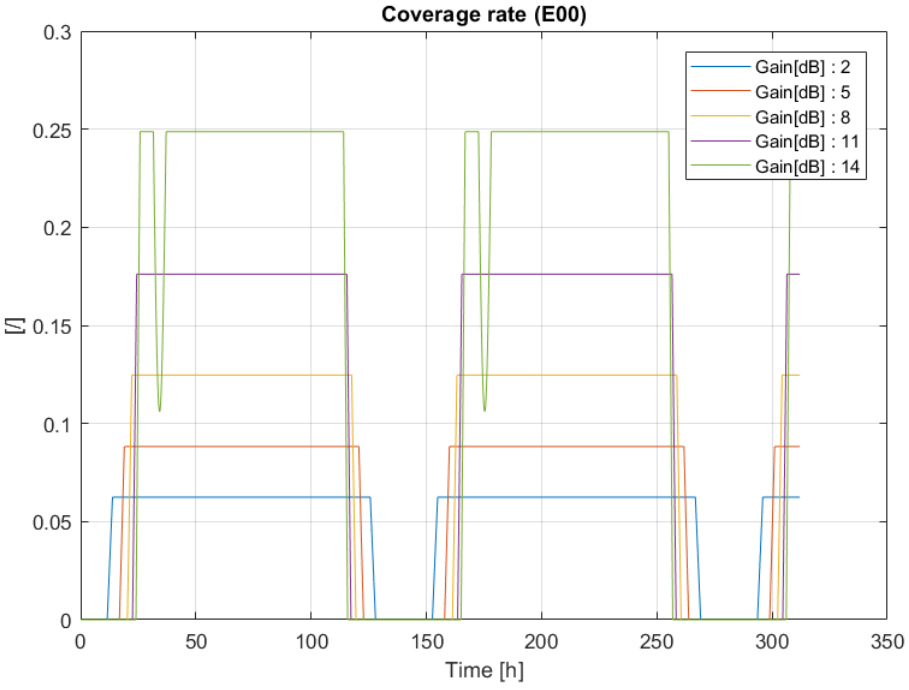

Figure 4.3: Coverage rate for multiple gains during an equatorial orbit.

One should note that once the beamwidth is known, the noise temperature model may be further improved regarding the polar orbit. Figure 4.4 shows the coverage S_1 surface of the beam by Neptune.

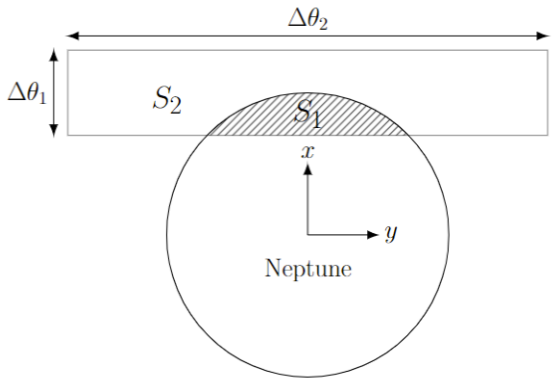

Figure 4.4: Coverage with known beamwidth.

The beam is approximated by a rectangle of surface S_2, its width is $\Delta\theta_2$ and its height is $\Delta\theta_1$. The coverage surface S_1 can easily be obtained by integrating the beam rectangle over the circle (representing Neptune) in the x direction. The noise temperature T_S can then be computed as :

$$T_S = \frac{1000S_1 + 200S_2}{S_{tot}} \tag{4.9}$$

with $S_{tot} = S_1 + S_2$.

4.5 Parametric analysis of the SNR: equatorial orbit

The goal of this section is to analyze the impact of different parameters (gain, time, bandwidth) on the SNR.

Bandwidth of 30 Hz Figure 4.5 illustrates the allure of the SNR with respect to time for a fixed power of 2.5 W and for different gains.

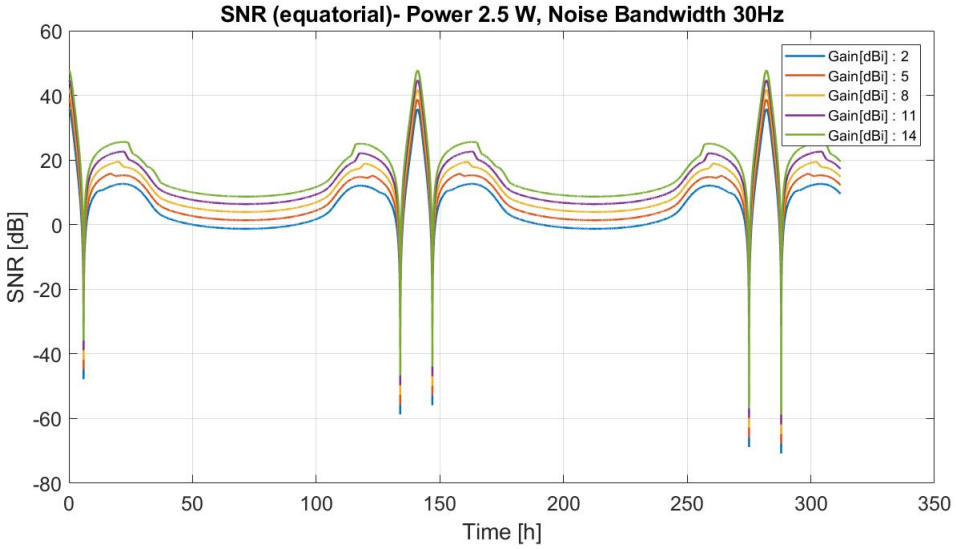

Figure 4.5: SNR for an equatorial orbit; bandwidth of 30 Hz and power of 2.5 W.

It can be seen that for gains larger than 5 dBi, and for positive elevations, the SNR is always larger than 0 dB. Note that we are not interested in the path of the orbit corresponding to negative elevations because the orbiter is behind Triton.

Bandwidth of 2.975 kHz In this case, if a SNR larger than 0 dB is required during the entire orbit, higher gains must be considered. Indeed, we lose 19.96 dB in the SNR as compared to the SNR model based on a bandwidth of 30 Hz .

Figure 4.6 shows the allure of the SNR with respect to time for a fixed power of 2.5 W and for different gains.

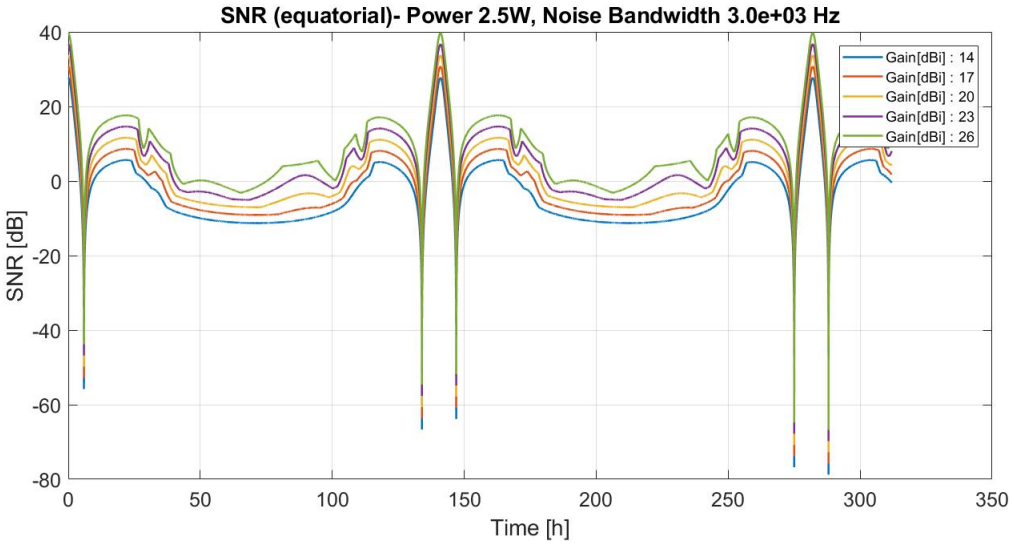

Figure 4.6: SNR for an equatorial orbit; bandwidth of 2.975 kHz and a power of 2.5 W

It can be seen that if the gain is lower than 23 dBi, it is not possible to have a SNR larger than 0 dB during the entire orbit. A less regular behavior of the SNR is also observed for increasing gains. This is due to the faster variations of the noise temperature.

Bandwidth of 295 kHz Again, the SNR for a 295 kHz bandwidth is 19.96 dB lower than that based on a bandwidth of 2.975 kHz. Figures 4.7a and 4.7b illustrate the SNR during a limited part of the orbit for powers of 6 W and 8 W respectively.

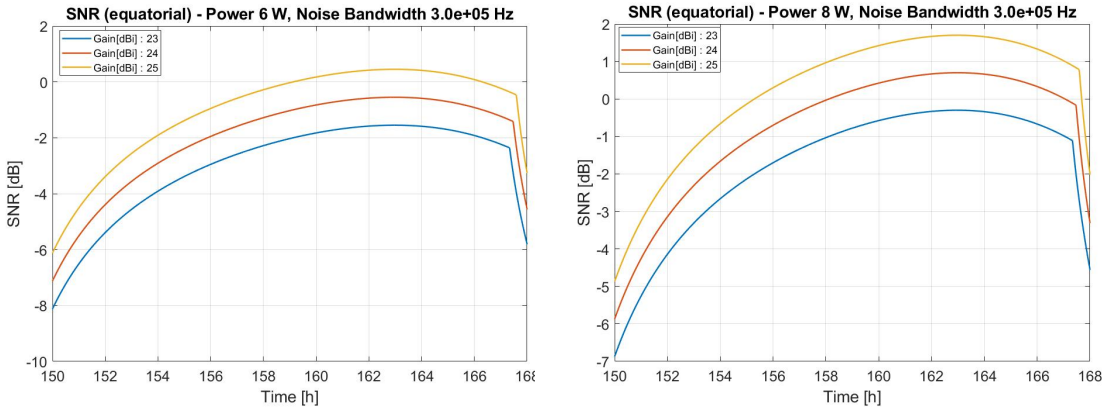

(a) (b)

Figure 4.7: SNR during a limited part of the orbit; bandwidth 295 kHz for powers of 6W in (a) and 8W in (b)

If we directly focus on the most efficient time window of the SNR, we note in Figures 4.7a that with a power of 6 W and a gain of 25 dBi, we could correctly communicate (SNR>0) during 3 hours. Whereas, as shown in Figure 4.7b, with a power of 8 W and a gain of 25 dBi it is possible to have a positive SNR during 6 hours while a 24 dBi gain allows 4 hours of communication.

4.6 Parametric analysis of the SNR: polar orbit

Bandwidth of 30 Hz Figure 4.8 illustrates the the SNR with respect to time for a fixed power of 2.5 W and for gains ranging from 2 dBi to 14 dBi.

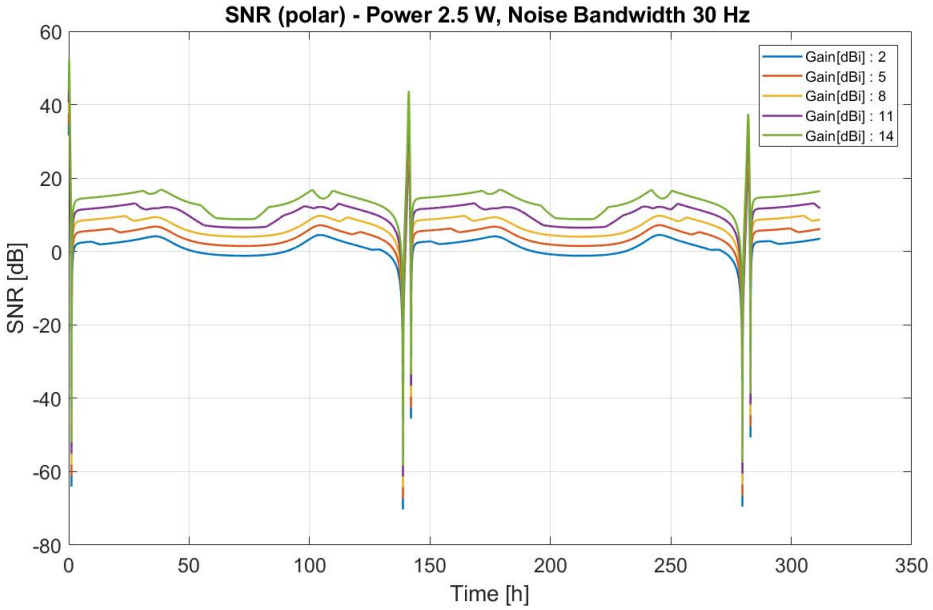

Figure 4.8: SNR for a polar orbit; bandwidth of 30 Hz and power of 2.5 W.

It can be observed that gains from 5 dBi up to 14 dBi, guarantee a positive SNR.

Bandwidth of 2.0881 kHz Figure 4.9 shows the SNR with a fixed power of 2.5 and for higher gains ranging from 14 dBi to 26 dBi.

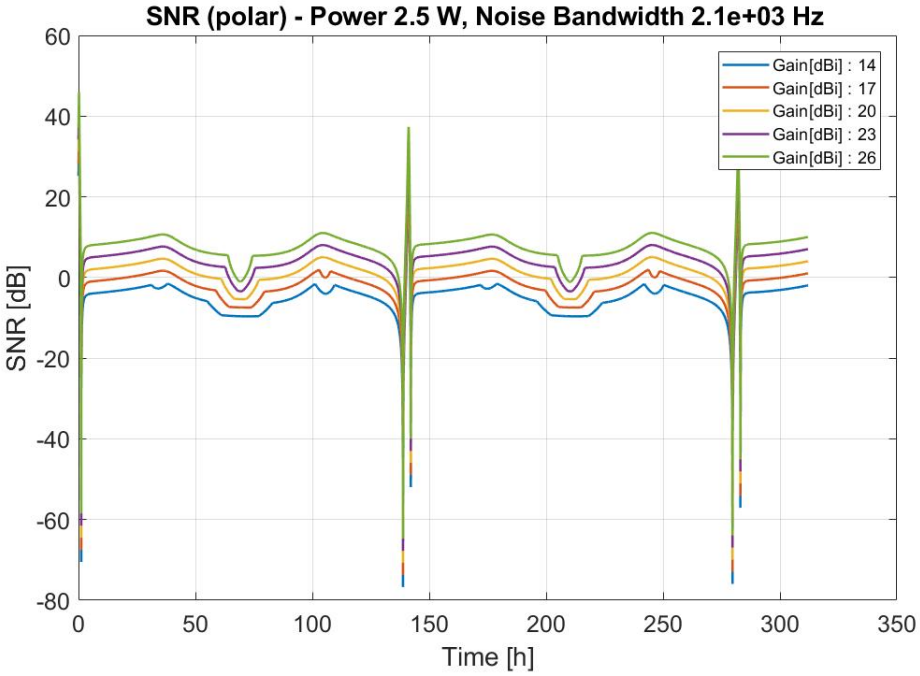

Figure 4.9: SNR for a polar orbit; bandwidth of 2.0881 kHz and a power of 2.5 W

We can see that only gains up to 20 dBi allows a SNR higher than zero during during a large part of the orbit. The sporadic variations at approximately time= 210 h and time= 240 h are more pronounced for the highest gains. They are due to the noise temperature variations.

Bandwidth of 145.34 kHz Figure 4.10 illustrates the time varying SNR for three different gains (23 dBi, 24 dBi and 25 dBi) and for a power of 8 W. We can see that the SNR is always under 0 dB, thus a good communication is not possible.

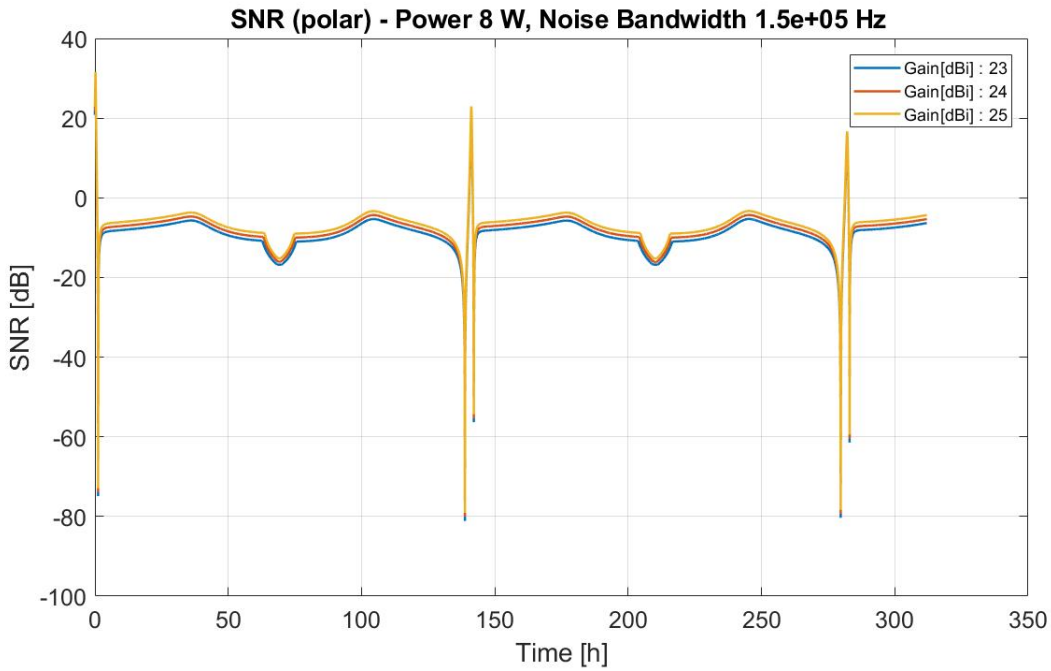

Figure 4.10: SNR for a polar orbit; bandwidth of 145.34 kHz and power of 8 W.

Chapter 5

Antenna Requirements

Space antennas must be able to withstand the harsh conditions of the space environment. They have to be robust so as to resist to radiation, extreme temperatures or mechanical stresses. Additionally, they should have enough gain in the directions of interest in order to relieve the power requirements [10].

One of the first requirements that should be considered is the material used to build the antenna. The use of dielectrics is strongly unadvised due to the cryogenic temperature on Triton and the cosmic radiations. Indeed, the dielectric properties of usual materials at such extremely low temperature (38 K) are unknown. Furthermore, the low conductivity of dielectrics can lead to the accumulation of electrons over time which could potentially cause electrostatic discharge events. That is the reason why the antenna should be made of metal only. All-metal antenna are very robust in this kind of harsh environment [9].

The mass and the size represent also a constraint in the design. Landers have limited space and resources. Therefore the size and mass of the antenna must be carefully balanced with other requirements of the mission. In this design, we have managed to reduce the size in terms of the gain requirement.

The polarization of the antenna should be circular. The main advantage of the circular polarization is that it is less sensitive to the changes in the orientation of the antenna (which may be caused by the movement of the lander for example) than the linear polarization. Indeed, a linearly polarized wave presents an electric field oscillating in a given plane along the direction of propagation. Consequently, the receiving linearly polarized antenna must be properly aligned to avoid a strong polarization mismatch. This dependence in antenna orientation makes the linear polarization more subject to fluctuations in the signal amplitude. The circular

polarization, on the other hand, has an electric field which oscillates in a circular way in the plane orthogonal to the direction of propagation, allowing to maintain a stable signal as there is no dependence with the orientation of the antenna. Circular polarization is also less sensitive to interferences from reflections. It is a good point because the Triton surface is likely reflective due to the major presence of water ice.

The considered bandwidth results from the maximum relative radial velocity, as calculated from the Doppler effect (see Section 4.4.1). The maximum bandwidth is 295 kHz and 145 kHz for the equatorial orbit and the polar orbit respectively.

Concerning the desired gain and the elevation sector of illumination of the antenna, it should be derived based on the SNR models and graphs of Chapter 4. In the present chapter and in the following of the work, a noise bandwidth of 30 Hz will be assumed.

Equatorial case Requiring a SNR higher than 0 dB, Figure 4.5 shows that a minimum gain of 5 dBi is required. Since Figure 4.5 has been obtained based on some approximations, we have added a margin of 3 dB, leading to a desired gain of 8 dBi. We have to consider the elevations and azimuths corresponding to the equatorial orbit. Considering that for scientific reasons, one is interesting in higher Doppler signatures, high elevations should be prioritized, keeping in mind that if the entire orbit can be covered (except when the orbiter is behind Triton of course), it is a plus. Figure 5.1 represents the elevation as a function of the time, along the equatorial orbit. One can easily see that a minimum elevation window $\theta_c \in [73°, 90°]$ is required. It corresponds to a θ in the range of $[0, 17°]$. Regarding the azimuth ϕ, its behavior is binary, taking the values of 90° or 270°.

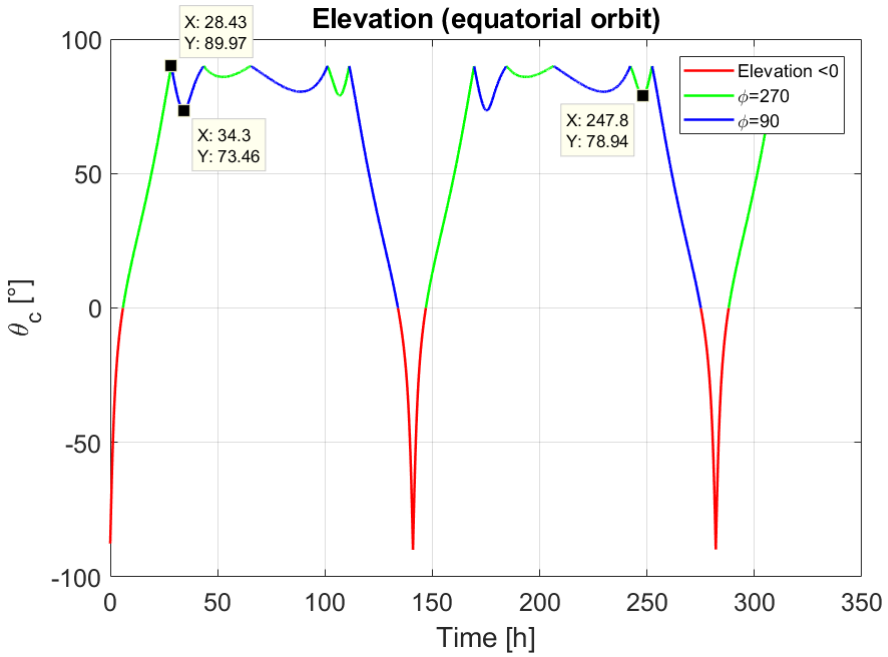

Figure 5.1: Elevation during the equatorial orbit. In red: the spacecraft passes behind Triton, it is not a zone of interest. In blue: the azimuth is equal to 90°. In green: the azimuth is equal to 270°.

Polar case Looking at Figure 4.8, it is understood that the gain requirements are the same as for the equatorial case. The elevation sector θ_c we will try to cover here range from 61° to 89° as shown in Figure 5.2. Based on Figure 5.3, it can can be seen that the azimuth varies gradually between 0° and 360°. Therefore, the antenna beam should cover a large azimuth sector.

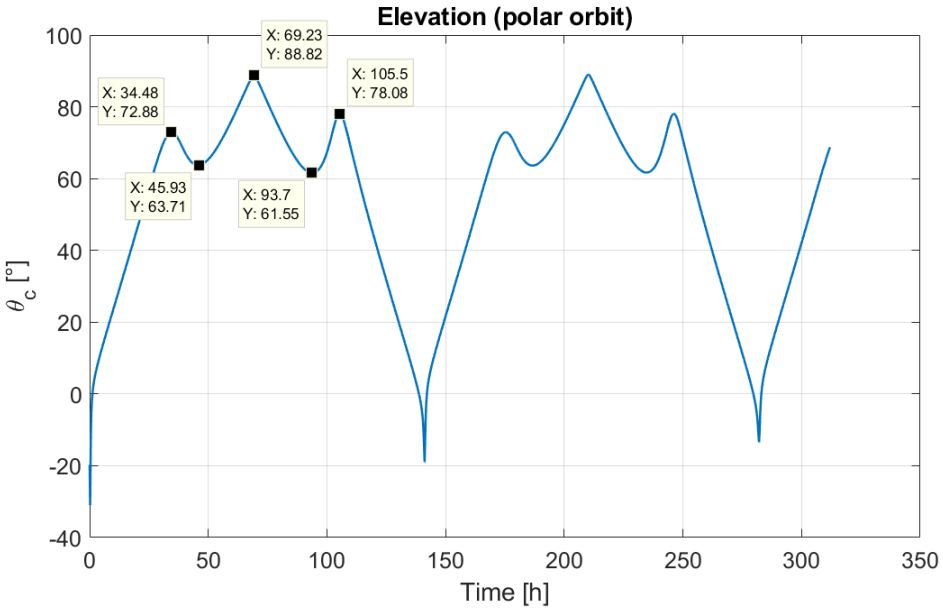

Figure 5.2: Elevation during the polar orbit.

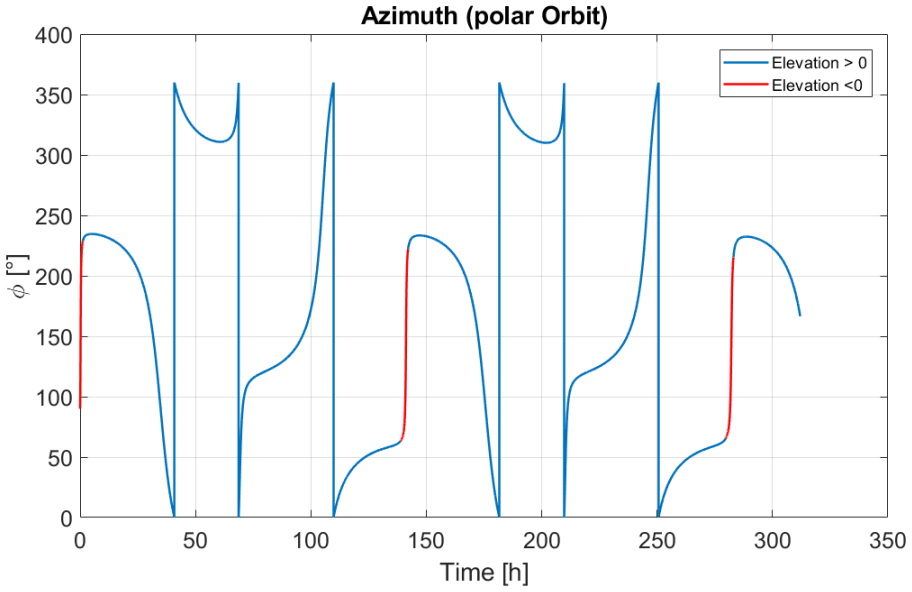

Figure 5.3: Azimuth during the polar orbit. In red: the elevation is negative, it is not a zone of interest.

	Type of orbit			
	Equatorial		Polar	
Parameter	Value	Unit	Value	Unit
Material	All-Metal	-	All-Metal	-
Maximum Mass	126	g	126	°
Frequency	8.45	GHz	8.45	GHz
Bandwidth	295.02	kHz	145.34	kHz
Polarization	RHCP	-	RHCP	-
Axial Ratio	5	dB	5	dB
Azimuth Range	90 or 270	°	[0, 360]	°
Minimal Elevation Range	[73, 90]	°	[61, 89]	°

Table 5.1: Antenna requirements.

Chapter 6

Antenna Design: unit cell analysis and optimization

The design of the antenna is mainly inspired by two designs, from [15] and [9]. Both designs achieve a circular polarization with a proper shape of the 3D unit cell.

The final design of the antenna unit cell consists in a bounded monopole placed on a square ground plane, as shown in Figure 6.1 with two different views. The monopole is aligned horizontally to the ground plane allowing a broadside radiation. The antenna is specifically composed of a cylindrical foot that serves as the feed. The foot is attached to a rectangular monopole lying parallel to the ground plane. The monopole curves from a parallelepipedic section to form a half-circle and is connected to the ground by a tip. The feed on the bottom of the foot is modeled as a delta-gap source, a type of radio frequency source which enables the generation of high-frequency RF signal by means of a spark discharge across a small gap (the delta gap).

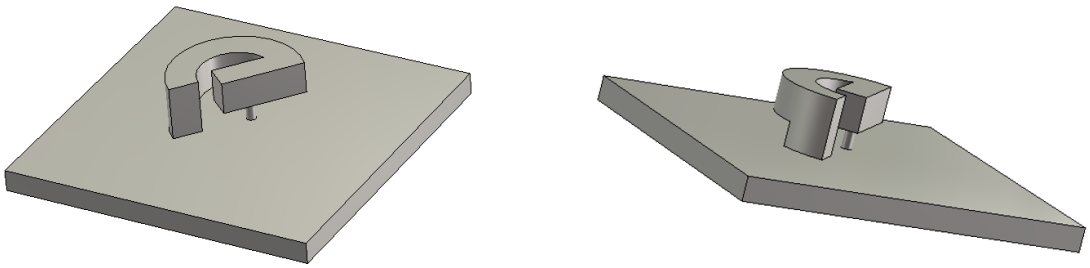

(a) (b)

Figure 6.1: 3D views of the curved monopole inspired from [15] and [9]

In order to meet the requirements of Chapter 5, we want to design a unit cell radiating as best as possible in the sector of interest, with a good polarization purity. For the equatorial orbit, the desired sector corresponds to an elevation ranging from 0° to 17° and for azimuths $\phi \in \{$ 90°, 270°$\}$. The unit cell has been optimized accordingly. The optimization parameters are listed in Table 6.1 and represented in Figure 6.2.

Parameters	Optimized Values
R_f	7.29 mm
H_f	2.32 mm
R_{in}	4.05 mm
R_{out}	7.293 mm
L_b	2.03 mm
α_{tip}	35°
L_g	35.5 mm
E	1.5 mm
delta gap	0.1 mm

Table 6.1: Parameters describing the curved monopole. H_f is the height of the foot and E is the thickness of the monopole.

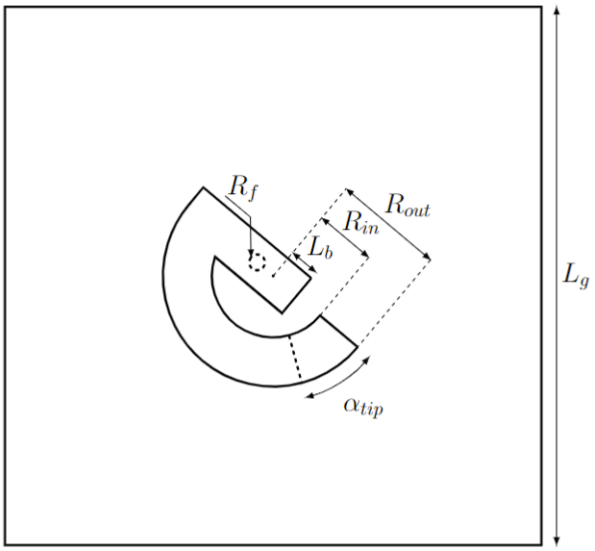

Figure 6.2: Sketch of the curved monopole. R_f is the radius of the foot, R_{in} and R_{out} are the internal and external radii of the circular part respectively, L_b is the distance from the edge of the parallelepiped to the center, α_{tip} is the angle over which the tip extends. L_g is the ground size.

The 3D copolar gain of the optimized unit cell is shown in Figure 6.3. The cut of the copolar gain in the plane $\phi \in \{90°, 270°\}$ is shown in Figure 6.4. Ideally, the pattern should have a maximum at $\theta = 0°$ and be symmetric around the broadside direction. However, it has been observed that bringing the maximum close to the broadside comes with a degradation of the polarization purity. Therefore a compromise should be found between the polarization purity and the direction of the main lobe. Figure 6.5 shows the evolution of the axial ratio. As can be seen, the axial ratio is quite good (< 5 dB) in almost all the sector, except for $\theta \in$ [-17°, -6°]. Finally Figure 6.6 provides the S_{11} as a function of the frequency; showing the good matching of the antenna.

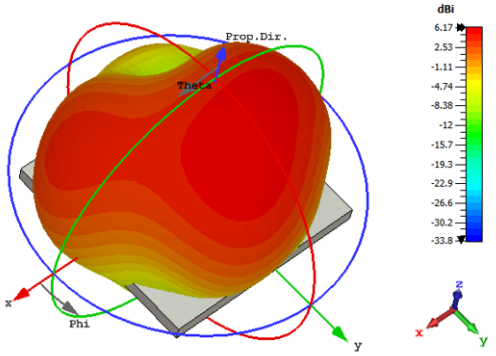

Figure 6.3: Copolar gain of the curved monopole in a cut at ϕ=90°.

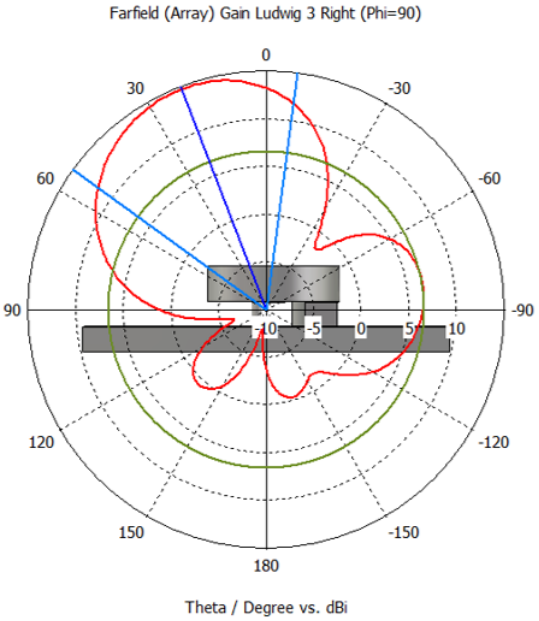

Figure 6.4: Copolar gain of the curved monopole in a cut at ϕ=90°.

Parameter	Unit	Value
Frequency	GHz	8.45
Main lobe amplitude	dBi	14.7
Main lobe direction	°	21
Angular width (3 dB)	°	61.6
Side lobe level	dBi	-8.1

Table 6.2: Characteristics of the beam obtained for the curved monopole in a cut at ϕ=90°.

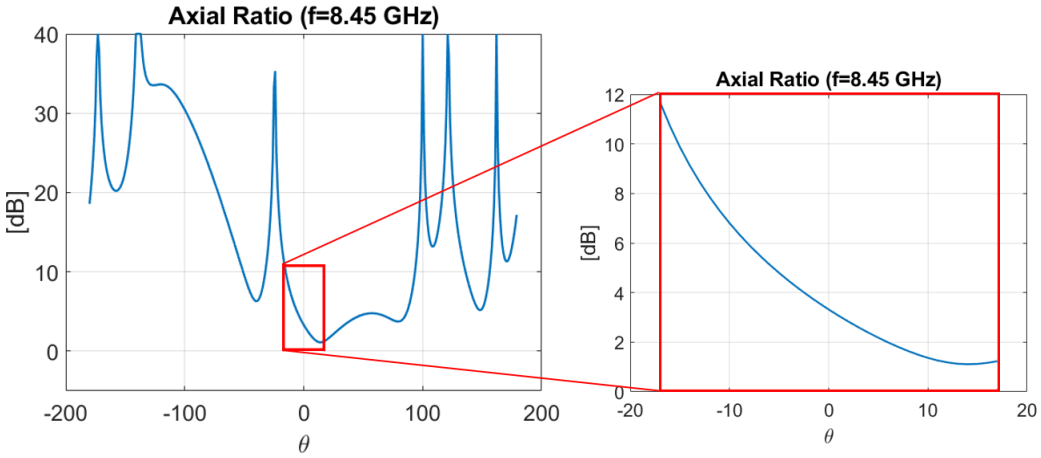

Figure 6.5: Axial ratio of the curved monopole at f=8.45 GHz. Right: a zoom on the theta angles of interest for the equatorial orbit.

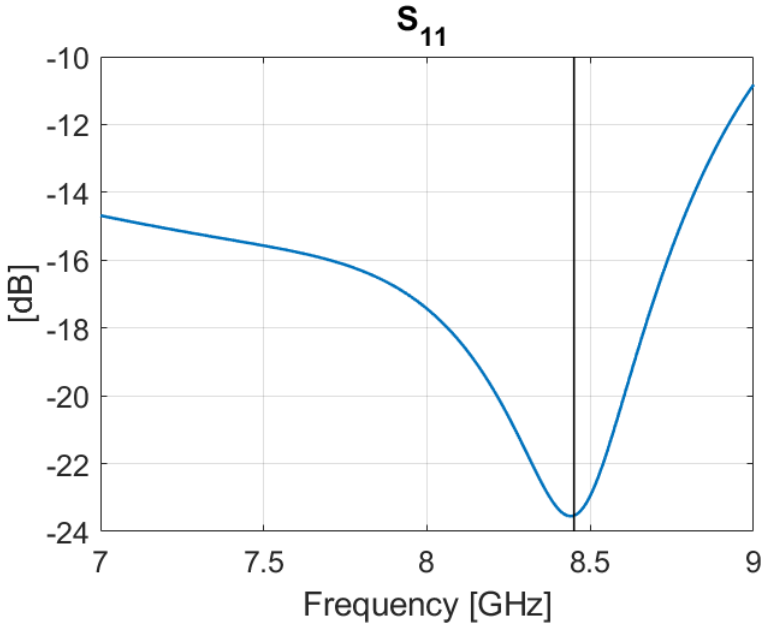

Figure 6.6: S_{11} parameter of the curved monopole

As shown in Chapter 5 for the polar orbit, the radiation sector of interest is $\theta \in [1°, 29°]$. That means, the beam needs to be oriented symmetrical around $\theta = 0°$ with a beamwidth approximately equal to 58°. We have observed that the unit cell optimized for the equatorial orbit satisfies more or less this requirement. Therefore the equatorial orbit unit cell will be used for the polar orbit.

Chapter 7

Antenna array devoted to the equatorial orbit

As previously explained in Section 3.2, the problem for the equatorial orbit can be reduced to a 2D problem. Indeed, the azimuth is binary, the orbiter orbits in the equatorial plane of Triton.

Therefore, one solution is to confine the beam towards the equatorial plane of Triton, i.e the beam has to be large in the equatorial plane and narrow in any plane orthogonal to the equatorial plane. In addition, it must have a minimum opening of θ= 17° on either side of the z-axis and therefore a total minimum beamwidth of 34° in elevation. Ideally, the beam should be symmetrical on either side of the zenithal z-axis so that the coverage of the elevations at ϕ= 90° is identical to that at ϕ= 270°.

The designed antenna is a uniform linear array consisting of N elements. The antenna is in the xy-plane with its axis aligned in the x-direction. The chosen number of elements results from the compromise between the antenna size and the minimum required gain (8 dBi). First, the copolar gain has been estimated while neglecting the coupling between unit cells. From array theory, the radiation pattern in absence of coupling can be written as:

$$F(\theta,\phi) = f(\theta,\phi)\sum_{n}^{N} a_n e^{j(n-1)(kdsin\theta cos\phi+\psi)} \tag{7.1}$$

where $f(\theta,\phi)$ is the unit cell pattern, ψ is the phase shift between consecutive elements, $k = 2\pi/\lambda$ with λ being the free-space wavelength, and a_n is the feeding

amplitude corresponding to the n-th element. For simplicity of the feeding network, we have chosen a_n=1. Finally, d is the inter-element distance. In this work, $d = \lambda/2$ to avoid exciting grating lobes, while maintaining a good effective aperture. Figure 7.1 shows the minimum gain in the sector of interest ($\theta \in$[-17°: 17°]) as a function of the number of elements N.

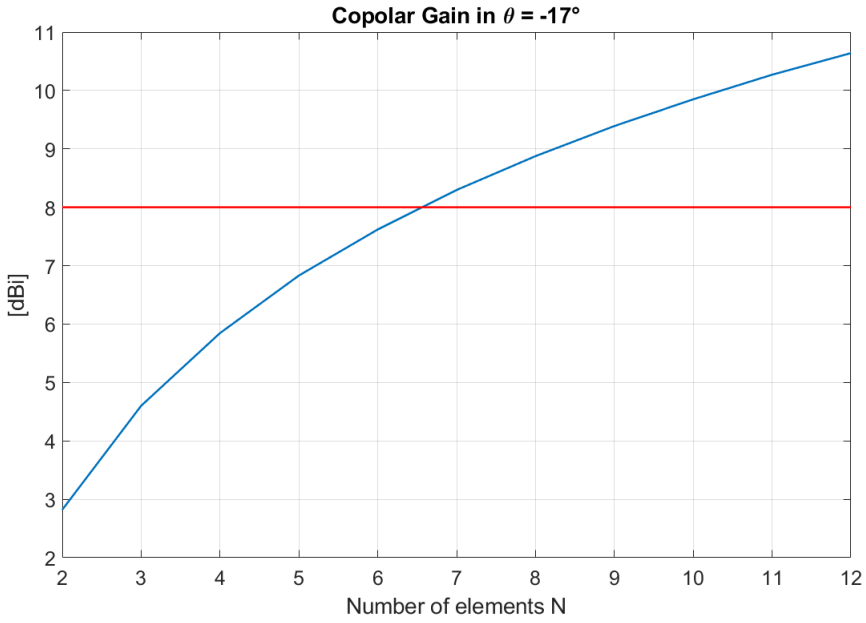

Figure 7.1: Minimum copolar gain in the sector of interest.

A minimum of 7 elements satisfies our gain requirements. However, we have decided to choose N=8 so as to have a significant margin.

7.1 Full-wave validation

In the previous section, the number of elements in the array has been optimized while neglecting the coupling effect. In this section, the designed array is validated using a full-wave model of CST. Figures 7.2 and 7.3 show the 3D copolar gain as well as its cut in the plane ϕ=90°. Table 7.1 lists the beam characteristics in the plane ϕ =90°. As can bee seen, we achieved a gain larger than 8 dBi in the sector of interest ($\theta \in$[-17°, 17°]).

The obtained gain is significantly higher than 8 dBi within the range $\theta \in$ [0, 17°]

with $\phi \in \{90°, 270°\}$. Indeed, the 3 dB angular beamwidth, which defines the sector for which the gain is larger than 11.5 dBi is $\theta \in$ [-32.4°, 58.4°].

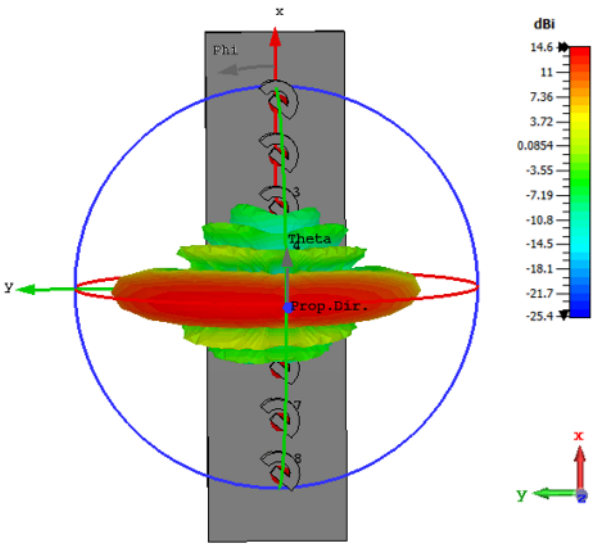

Figure 7.2: 3D representation of the beam obtained with a full-wave model of CST.

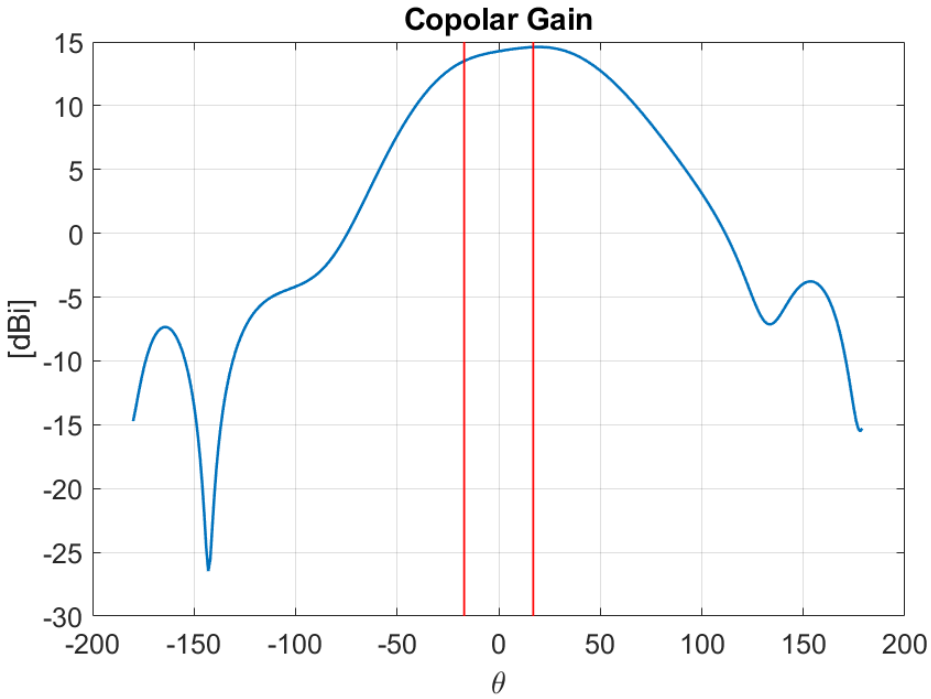

Figure 7.3: Copolar gain in the plane ϕ= 90° obtained with a full-wave model of CST.

Parameter	Unit	Value
Frequency	GHz	8.5
Main lobe amplitude	dBi	14.6
Main lobe direction	°	20
Angular width (3 dB)	°	90.8
Side lobe level	dB	-18.4

Table 7.1: Characteristics of the beam obtained for the equatorial orbit for a cut at ϕ=90°.

The gain as a function of the time on the equatorial orbit is represented in Figure 7.4. As expected, we have a very low gain for negative elevations. It is worth mentioning that we are not interested in the negative elevations because it is the moment when the spacecraft is behind Triton. Moreover, it is observed that the allure of the gain is not symmetrical with respect to the azimuth ϕ. This is due to the asymmetry of the unit cell pattern (see Figure 6.4).

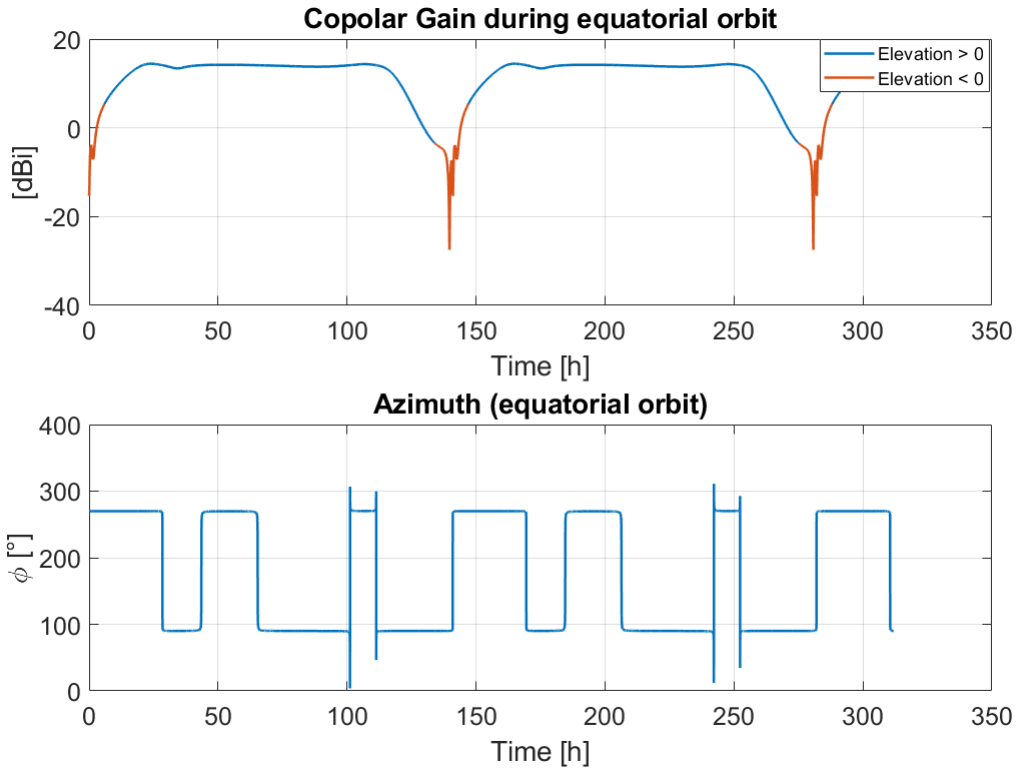

Figure 7.4: Gain provided by the antenna array during the equatorial orbit and the corresponding azimuth.

7.2 Analysis of the SNR

Once the gain computed at each point on the equatorial orbit, the resulting SNR can be derived using the method explained in Chapter 4. Figure 7.5 compares the obtained SNR with that corresponding to an antenna providing 8 dBi gain. One should note that, in opposite to the approximate model used in Section 4.4.2 for the noise temperature calculation, here, the real beamwidth 90.8° and the maximum direction θ_{max}= 20° can be used. It can be seen that in almost the entire orbit, the SNR is larger than that obtained from the 8 dBi gain antenna except close to the regions corresponding to negative elevations.

Finally, it is useful to look at the elevations for which the SNR is larger than zero during the orbit. In Figure 7.6, we can see that when we are on the left of the part of the curve for which the elevation is negative, i.e. just before the orbiter

passes behind the lander (Triton), an SNR larger than zero is guaranteed up to an elevation of 11°. Then, once the orbiter is again visible in the sky of the lander after passing behind Triton, the SNR is positive from an elevation of 3° as indicated by the data tips in Figure 7.6. Again, this difference in value is explained by the previously mentioned asymmetry of the unit cell pattern. We can therefore conclude that this design allows us to cover almost the entire orbit while having an SNR significantly larger than zero for high elevations and therefore a very good link quality between the lander and the orbiter. It is clear that these results exceed our initially set goal.

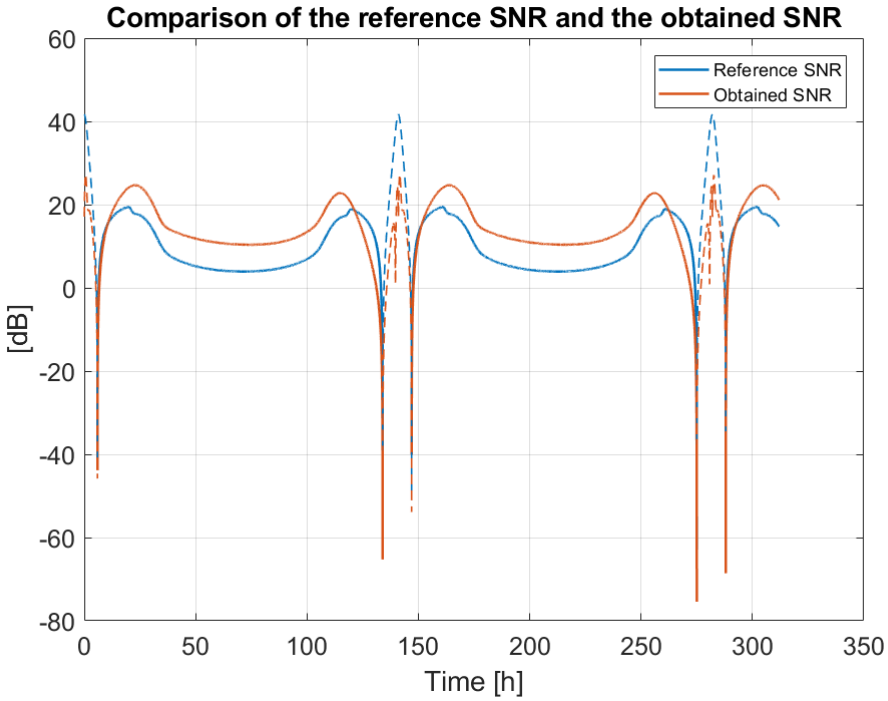

Figure 7.5: SNR versus time on the equatorial orbit. The obtained SNR after antenna design is compared to a reference. The reference corresponds to an antenna providing a 8 dBi gain in the sector of interest. The dashed lines refer to negative elevations.

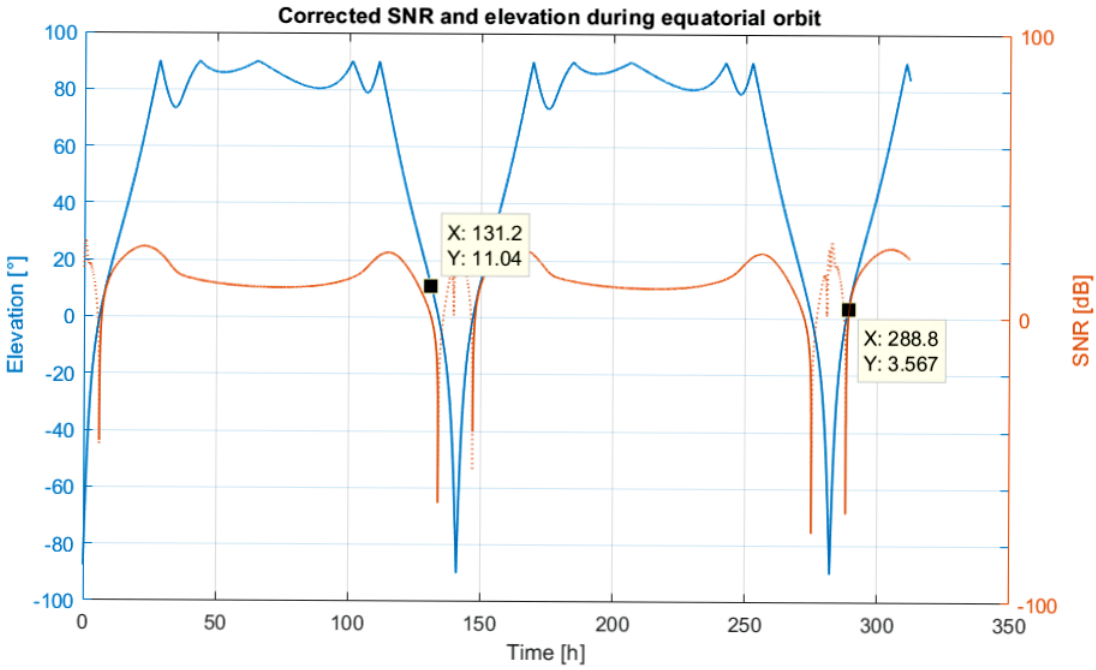

Figure 7.6: Obtained SNR and elevation on the equatorial orbit. The datatips correspond to the elevation at which the SNR is 0 dB. Negative elevations are not interesting because it is the moment when the spacecraft passes behind Triton.

Chapter 8

Polar orbit array

Unlike the equatorial orbit, the polar orbit cannot be reduced to a 2D problem. Indeed, the plane in which the spacecraft orbits is now perpendicular to the equatorial plane as represented in Figure 3.5.

The main difficulty is, as analyzed in Chapter 5, the variation of the azimuth. Starting from the equatorial orbit design, which provides a wide beam in the equatorial plane, it can be seen that steering the beam with respect to θ along the axis of the array will enable a significant coverage of the polar orbit. Therefore, the equatorial orbit design can still be used provided that a beam scanning is implemented in elevation. In this work, the scanning is carried out electronically by imposing a linear phase evolution in the array. This type of antenna is commonly called a phased array [16].

A well known solution for phasing the array consists of using a beamforming network. Several beamformers exist, among which the Blass matrix, the Nolen matrix and the Butler matrix [17]. Here, we have chosen a Butler matrix due to its simplicity and compactness [18]. Additionally, it is completely passive and does not require particularly terminated loads. A Butler matrix is a passive 2N network, with N inputs and N outputs. In transmitting mode, each output is connected to a given element of the antenna array. Depending on the selected input port, a particular linear phase shift evolution is impressed on the array. Figure 8.1 shows the block diagram of a 8x8 Butler matrix. The beamformer is implemented with 90° hybrid couplers, crossovers and fixed delays lines. In our work, the Butler matrix is modeled at system level, which means that we introduce in the electromagnetic simulation of the antenna, the phase shifts generated by the Butler matrix. The phases introduced by the Butler matrix are summarized in Table 8.1. The phase

shift variation between consecutive elements is given by (8.1), where n=1:4 is the index of the symmetrical beam port.

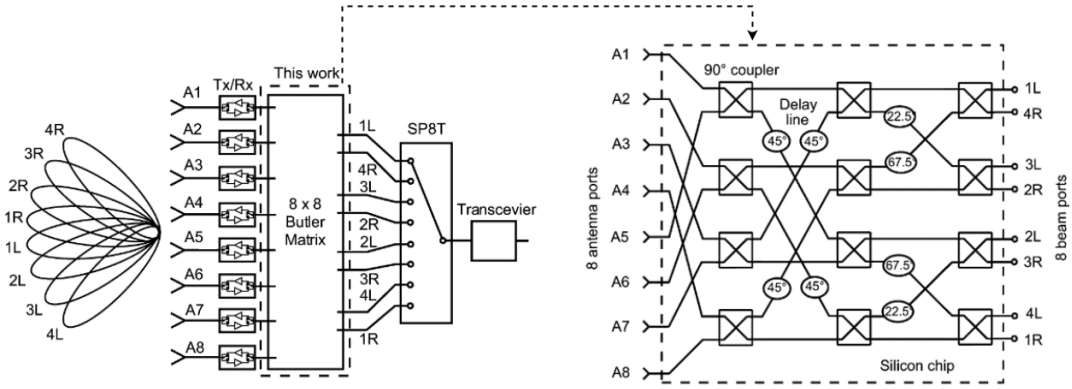

Figure 8.1: From [19], left: a conceptual diagram showing the layout of a 8x8 Butler matrix. Right: diagram of the circuit implementation.

$$\Delta\varphi = \pm\frac{(2n-1)\pi}{N} \tag{8.1}$$

	Beam ports							
Antenna Ports	1L	4R	3L	2R	2L	3R	4L	1R
A1	90	-180	157.5	-112.5	135	-135	157.5	-112.5
A2	112.5	-22.5	-90	-180	-157.5	112.5	-45	-135
A3	135	-135	22.5	112.5	-90	0	112.5	-157.5
A4	157.5	67.5	135	45	-22.5	-112.5	-90	-180
A5	-180	-90	-112.5	-22.5	45	135	67.5	157.5
A6	-157.5	112.5	0	-90	112.5	22.5	-135	135
A7	-135	-45	-112.5	-157.5	-180	-90	22.5	112.5
A8	-112.5	157.5	-135	135	-112.5	157.5	-180	90
$\Delta\varphi$	22.5	-157.5	112.5	-67.5	67.5	-112.5	157.5	-22.5
Beam Angle θ_x	-7	+61	-39	+22	-22	+39	-61	+7

Table 8.1: Phases applied to the different elements to produce a beam in a particular θ direction

Figures 8.2 and 8.3 show the 3D copolar gains corresponding to each beam port. A cut of the pattern in the plane ϕ= 0° is provided in Figure 8.4. We can see an asymmetry in the pattern when comparing positive elevations and negative ones. This is due to the initial asymmetry in the unit cell pattern.

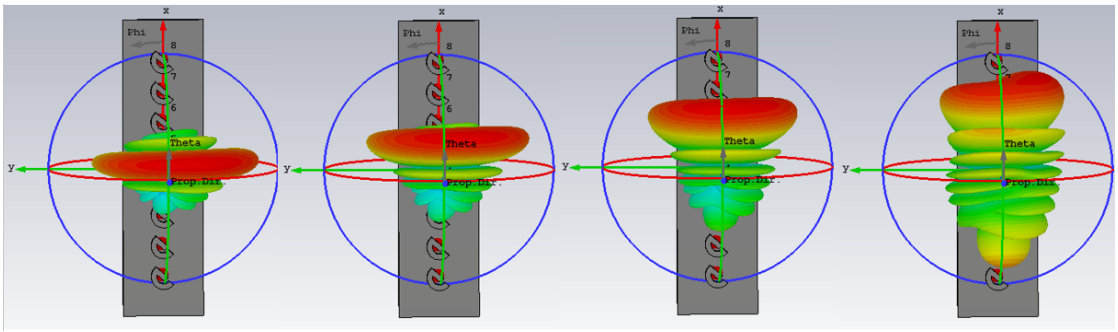

Figure 8.2: Copolar gain for negative phase shifts between the elements. From left to right the beams are oriented in $\theta = 7°, 22°, 39°, 61°$ respectively.

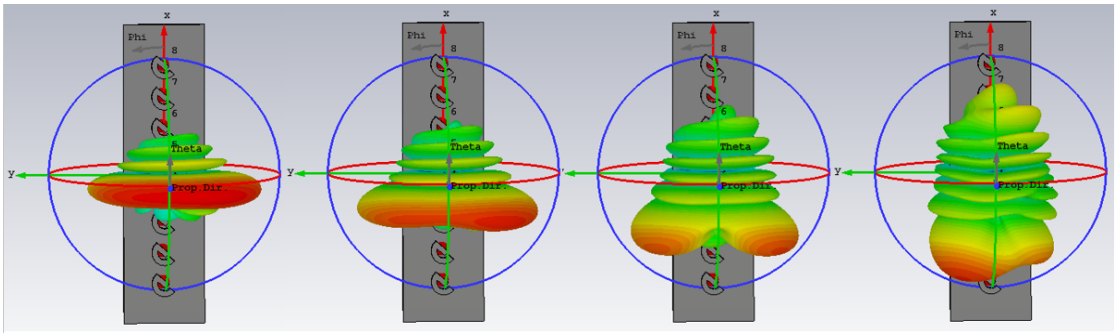

Figure 8.3: Copolar gain for positive phase shifts between the elements. From left to right the beams are oriented in $\theta = -7°, -22°, -39°, -61°$ respectively.

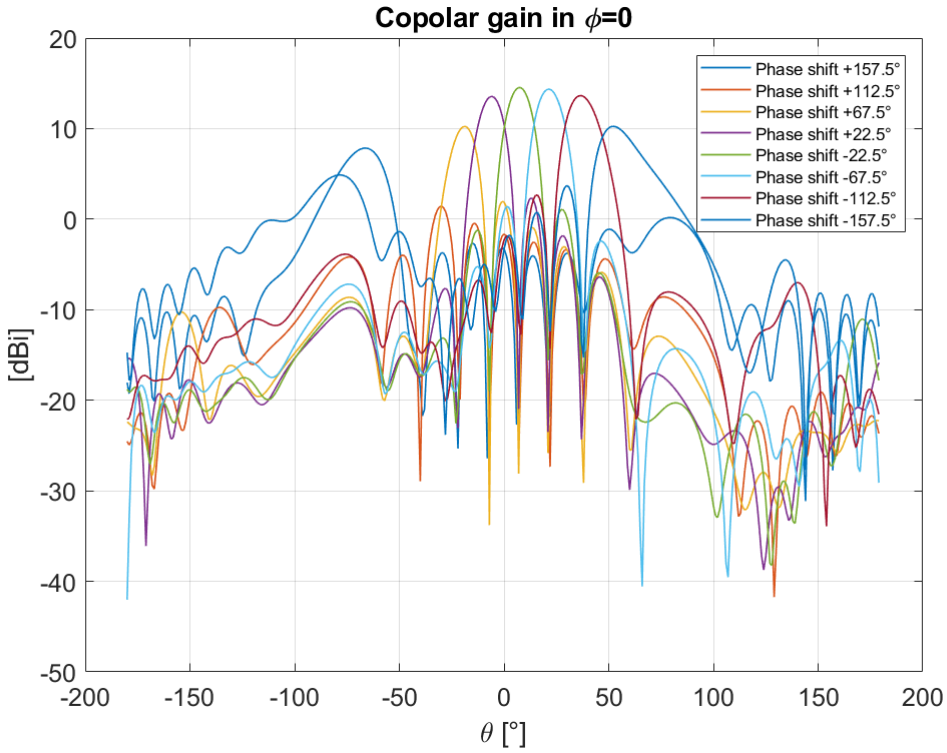

Figure 8.4: Cut of the copolar gain in the cut ϕ= 0° for different input ports of the beamformer.

Ultimately, similar to the equatorial case, it is useful to understand the gain profile over time, as it would allow us to see the SNR that we could achieve with this design. In order to optimize the link budget throughout the orbit, we select from the eight possible 3D patterns, the one that provides us the highest gain for the pair (θ, ϕ) of interest, i.e that corresponding to a given time t along the orbit. Doing so, the gain can be computed as a function of the time. This is represented in Figure 8.5.

We can distinguish bounces; they are caused by the change in the chosen beam pattern. The copolar gain is mostly above 8 dBi for high elevations, meeting our target of a minimum gain of 8 dBi.

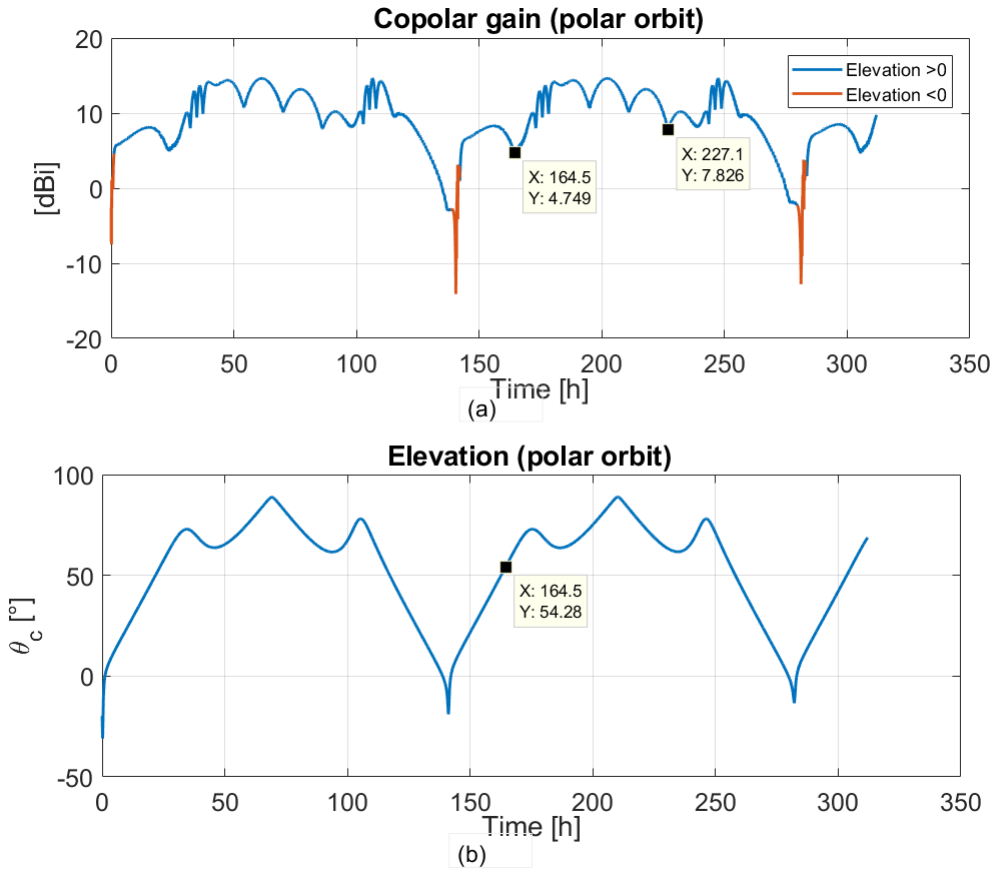

Figure 8.5: (a) Copolar gain obtained with the phased array (b) Elevation θ_c of the polar orbit.

Once the time-varying gain obtained, we inject it into the SNR model to have a more realistic SNR prediction. The lower gain obtained at low elevations should not be a major issue because low elevations usually correspond to smaller ranges. Figure 8.6 compares three results, namely the initially estimated SNR using a constant gain of 8 dBi, the SNR with the designed antenna, and the SNR with both the gain correction and the noise temperature calculation correction. The noise temperature correction is the one discussed in Section 4.4.2.

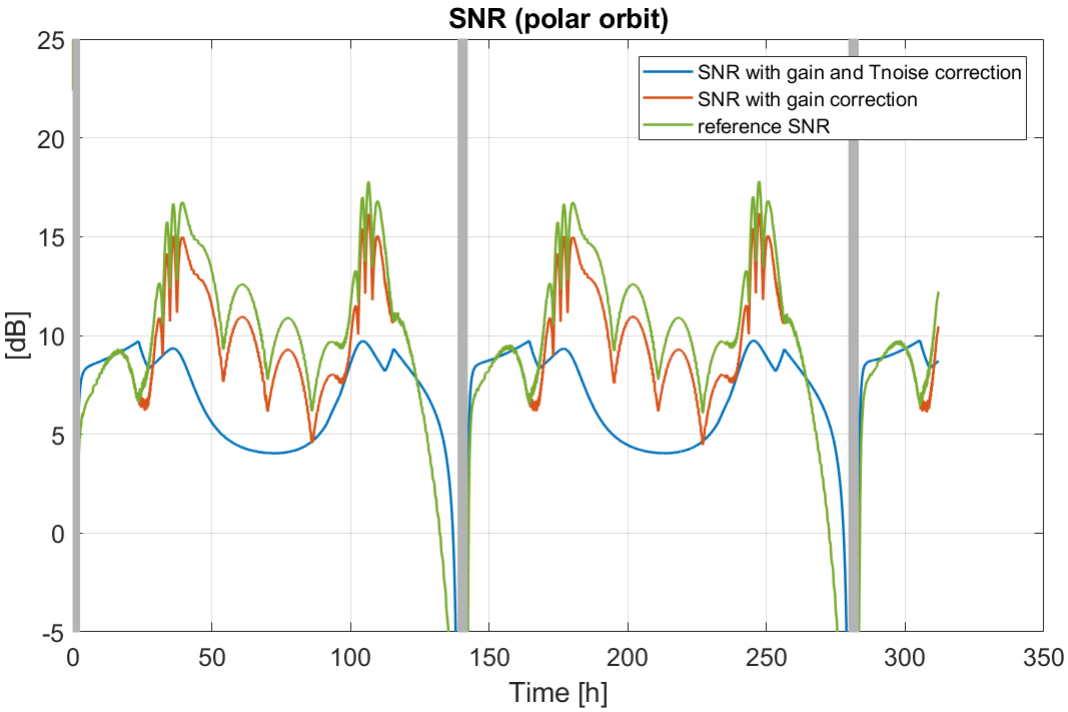

Figure 8.6: Comparison of the SNR during the polar orbit. Negative elevations are greyed out.

It is observed that there is a significant increase in SNR for the highest elevations when the designed antenna is used.

Finally, by analyzing Figure 8.7, we can see that a SNR larger than 0 dB is guaranteed up to an elevation θ_c of 16° just before passing behind Triton (left to the negative elevations). Then, just after its passage behind Triton, the lander can communicate with the orbiter again when the latter is at a relative elevation θ_c of 4°. This study shows that the orbit can be almost completely covered with a SNR that is significantly larger than 0 dB, thus demonstrating the quality of the link.

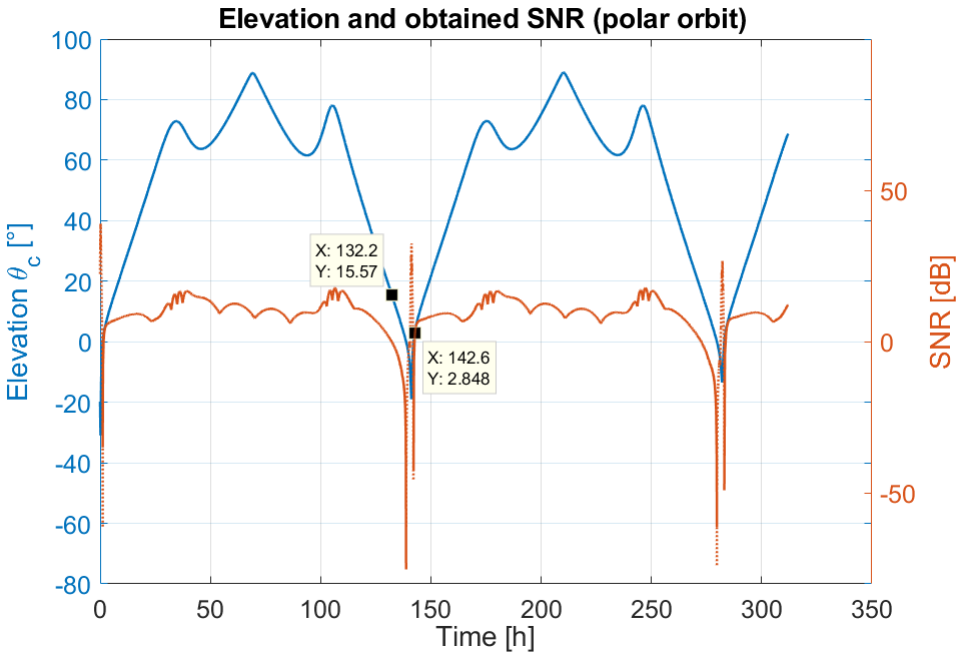

Figure 8.7: SNR and elevation versus time for the polar orbit.

Chapter 9

Conclusion

Triton is one of the moons of Neptune with a great scientific interest. Similar to what is carried out for Mars planet within the Lara project, this work aims at analyzing the interior of Triton through radio waves sensing. More specifically, we have studied the communication channel between a lander located on Triton and an orbiter around Neptune. Two orbital configurations have been considered, namely the equatorial orbit and the polar orbit. For each of the orbital configuration, a detailed study of the link budget has been carried out. This has allowed us to derive the antenna requirements.

A metal-only linear antenna array has then been proposed to satisfy the communication needs. The linear array is made of 8 elements. For the equatorial orbit, the antenna is designed and disposed so as to focus its power towards the equatorial plane, while maintaining a large beamwidth within this plane. As small elevations usually correspond to smaller distances, the decrease of the antenna gain for small elevations is compensated by the decrease of the range. Consequently, the Signal to Noise Ratio (SNR) can be maintained relatively constant and large enough over a large portion of the orbit.

For the polar orbit, it has appeared that the equatorial orbit antenna can still be used provided that beamforming is implemented so as to cover the portion of the orbit not being in the equatorial plane. In this work, we have proposed the use of a Butler matrix beamformer. The numerical analysis of the SNR shows a less stable behavior in time as compared to the equatorial case. Indeed, due to the discrete possible directions of the beam enabled by the beamformer, bounces in the SNR are inevitable. Nevertheless, the SNR is maintained sufficiently high enough over almost the entire orbit.

9.1 Future work

- Our study has been limited to the case of two particular orbits and a specific position of the lander. Other orbits and lander positions may provide better communication links. Future works may analyze and optimize the choice of the orbit.

- The proposed unit cell has not a symmetrical radiation pattern with respect to broadside. As a consequence, the allure of the SNR is not optimum. Future works may investigate other unit cells capable of radiating symmetrically around broadside while providing a good polarization purity.

- A beamforming network based on the Butler matrix has been used. As shown in the gain corresponding to each beam port, the maximum gain corresponding to each port varies significantly and the sidelobes are not well controlled. A beamformer that will be able to introduce phase shifts and amplitudes variations will certainly help to solve this issue. Such beamformer may for example be based on a flat metasurface. Therefore, future works may investigate the design of more complex beamformers.

Bibliography

[1] *The European Space Agency - Neptune.* https://www.esa.int/content/view/full/516386.

[2] *UNIVERSE TODAY- Space and astronomy news.* https://www.universetoday.com/22070/surface-of-neptune/.

[3] *How bright are our planets?* https://skyandtelescope.org/observing/measuring-planet-magnitudes/.

[4] Elizabeth Gibney. "RARE CHANCE TO REACH ICE GIANTS EXCITES SCIENTISTS". *Nature* 579, Mar. 2020.

[5] *Les satellites de glace.* http://planets.oma.be/ISY/neptune/triton.php.

[6] *Lander Lara Radio science.* https://lara.oma.be.

[7] Sumit Karki. "Design and Modeling of Circularly Polarized Conical Beam Antennas for Space Missions". PhD thesis. 2018.

[8] *How long would it take to get to Neptune?* https://theplanets.org/how-long-would-it-take-to-get-to-neptune/.

[9] Nacer Chahat, Brant Cook, Heather Lim, and Polly Estabrook. "All-Metal Dual-Frequency RHCP High-Gain Antenna for a Potential Europa Lander". *IEEE Transactions on Antennas and Propagation* 66.12, Dec. 2018.

[10] Chahat et al. Nacer. "Advanced cubesat antennas for deep space and earth science missions". *IEEE Antennas and Propagation Magazine* 61.5, Oct. 2019, pp. 37–46.

[11] *NASA solar system exploration.* https://solarsystem.nasa.gov/moons/neptune-moons/triton/by-the-numbers/.

[12] *Ice Giants CDF Study Report: CDF-187(C)*. ESA, 2019.

[13] Nicolas et al. Rambaux. "Rotation and libration of celestial bodies". *Journées Systèmes de Références*, Sept. 2018.

[14] Steve Oleson and Geoffrey Landis. *Triton Hopper: Exploring Neptune's Captured Kuiper Belt Object*. NASA, 2018.

[15] Thomas Pairon, Sumit Karki, Stefania Monni, and Christophe Craeye. "Efficient analysis of arrays of compact metallic elements devoted to satellite SAR". *13th European Conference on Antennas and Propagation (EuCAP)*, 2019.

[16] Constantine A. Balanis. *Antenna Theory Analysis and Design*. Third Edition. John Wiley Sons, 2016.

[17] Han et al Ren. "A Novel 2-D 3x3 Nolen Matrix for 2-D Beamforming Application". *IEEE Transactions on microwave theory and techniques* 67.11, 2019, pp. 4622–4631.

[18] Arshad Karimbu Vallappil, Mohamad Kamal A. Rahim, Bilal A. Khawaja, Noor Asniza Murad, and Mohammed Gajibo Mustapha. "Butler Matrix Based Beamforming Networks for Phased Array Antenna Systems: A Comprehensive Review and Future Directions for 5G Applications". *IEEE Access* 9, 2021, pp. 3970–3987.

[19] Berke Cetinoneri, Yusuf A. Atesal, and Gabriel M. Fellow Rebeiz. "An 8x8 Butler Matrix in 0.13- μm CMOS for 5–6-GHz Multibeam Applications". *IEEE Transactions on Microwaves Theory and Techniques* VOL. 59.NO. 2, 2011.

[20] N. A. Muhammad, S. K. A. Rahim, N. M. Jizat, T. A. Rahman, K. G. Tan, and A. W. Reza. "Beam Forming Networks Using Reduced Size Butler Matrix". *Wireless Personal Communications* 63, 2010, pp. 765–784.

[21] Theodoros N. Kaifas and John N. Sahalos. "On the design of a single-layer wideband butler matrix for switched-beam UMTS system applications". *IEEE Antennas and Propagation Magazine* VOL. 48.NO. 6, 2006, pp. 193–204.

[22] Chia-Chan Chang, Ruey-Hsuan Lee, and Ting-Yen Shih. "Design of a Beam Switching/Steering Butler Matrix for Phased Array System". *IEEE Transactions on Antennas and Propagation* VOL. 58.NO. 2, 2010.

UNIVERSITÉ CATHOLIQUE DE LOUVAIN
École polytechnique de Louvain
Rue Archimède, 1 bte L6.11.01, 1348 Louvain-la-Neuve, Belgique | **www.uclouvain.be/epl**